Title: Thermal history of the lower Carboniferous Culm Basin in the Nizky Jesenik Mts. (NE Bohemian Massif, Czech Republic and Poland)

Author: Dariusz Botor, Tomasz Toboła, Iwona Jelonek

Citation style: Botor Dariusz, Toboła Tomasz, Jelonek Iwona. (2017). Thermal history of the lower Carboniferous Culm Basin in the Nizky Jesenik Mts. (NE Bohemian Massif, Czech Republic and Poland). "Annales Societatis Geologorum Poloniae" (vol. 87 (2017), s. 13–40), doi 10.14241/asgp.2017.002

Annales Societatis Geologorum Poloniae (2017), vol. 87: 13–40. doi: http://dx.doi.org/10.14241/asgp.2017.002

THERMAL HISTORY OF THE LOWER CARBONIFEROUS CULM BASIN IN THE NÍZKÝ JESENÍK MTS. (NE BOHEMIAN MASSIF, CZECH REPUBLIC AND POLAND)

Dariusz BOTOR[1], Tomasz TOBOŁA[1] & Iwona JELONEK[2]

[1] AGH University of Science and Technology, Faculty of Geology, Geophysics and Environmental Protection, al. Mickiewicza 30, Kraków 30–059, Poland; e-mail: botor@agh.edu.pl; tob@geolog.geol.agh.edu.pl
[2] University of Silesia, Faculty of Earth Sciences, ul. Będzińska 60, Sosnowiec 41–200, Poland; e-mail: iwona.jelonek@us.edu.pl

Botor, D., Toboła, T. & Jelonek, I., 2017. Thermal history of the lower Carboniferous Culm Basin in the Nízký Jeseník Mts. (NE Bohemian Massif, Czech Republic and Poland). *Annales Societatis Geologorum Poloniae*, 87: 13–40.

Abstract: Raman microspectroscopy of organic matter, vitrinite reflectance and fluid inclusion data were used to reconstruct the thermal history in the lower Carboniferous accretionary prism of the Culm Basin in the Nízký Jeseník Mts. (NE Bohemian Massif). The model involves the Variscan (mid–late Carboniferous) burial diagenesis, which was overprinted by a post-Variscan, probably Permian and/or early Mesozoic, thermal pulse(s) in its central and western parts. The latter may have been related to advective heat transport and the circulation of hot fluids. In the siliciclastic rocks of the Culm Basin, the maximum palaeotemperatures varied from ~200 ± 30 °C in the E (in the Hradec-Kyjovice Formation) to ~350 ± 30 °C in the NW (in the Andělská Hora Formation).

Key words: Raman spectroscopy, carbonaceous material, maximum temperature, fluid inclusions, vitrinite reflectance, Culm Basin, Moravo-Silesian Fold and Thrust Belt.

Manuscript received 25 August 2016, accepted 3 May 2017

INTRODUCTION

The irreversible processes of coalification and graphitisation of organic (carbonaceous) matter (OM) make it possible to determine the degree of diagenesis and metamorphism in both sedimentary and very low- to low-grade metamorphic rocks (Teichmüller, 1987; Taylor *et al.*, 1998; Hartkopf-Fröder *et al.*, 2015). Dispersed OM, as a common component of sedimentary rock, is transformed progressively by rising temperature and pressure. The transformation of OM involves structural and compositional changes (e.g., Diessel and Offler, 1975; Diessel *et al.*, 1978; Teichmüller, 1987; Taylor *et al.*, 1998). Diverse temperature-sensitive parameters (e.g., vitrinite reflectance, Rock-Eval Tmax, clay minerals transformation, fluid inclusions, Conodont Alteration Index, etc.) have been applied over the last decades, providing insight into the thermal history of sedimentary rocks (e.g., Teichmüller, 1987; Yalcin *et al.*, 1997 and references therein; Taylor *et al.*, 1998; Hartkopf-Fröder *et al.*, 2015). One of the most widely used parameters is mean random vitrinite reflectance (VR_r), from which the maximum temperature can be estimated by assuming the controlling kinetic factors and knowing the subsidence history of the rock analysed (e.g., Sweeney and Burnham, 1990; Barker and Pawlewicz, 1994). Another method, which has gained interest in the last decade, is Raman microspectroscopy of carbonaceous (organic) material. This is particularly useful in the low-grade metamorphic range, where many other techniques (including VR_r) are not very precise (Beyssac *et al.*, 2002a; Rantitsch *et al.*, 2004; Rahl *et al.*, 2005; Lahfid *et al.*, 2010; Aoya *et al.*, 2010; Kouketsu *et al.*, 2014). A Raman spectrum of OM occurring in metasediments changes systematically with an increasing degree of metamorphism (e.g., Jehlička and Rouzaud, 1990; Pasteris and Wopenka, 1991; Wopenka and Pasteris, 1993; Jehlička *et al.*, 2003; Kwiecińska *et al.*, 2010; Morga, 2011, 2014; Kouketsu *et al.*, 2014). These changes are mainly controlled by temperature (Beyssac *et al.*, 2002a). By applying this method, temperatures in the range 330–650 °C (Beyssac *et al.*, 2002a) can be determined with a calibration-attached accuracy of ± 30 °C (Aoya *et al.*, 2010). Several authors also demonstrated that the evolution of the Raman spectra of OM in very low-grade metamorphism is strongly correlated with the peak temperature of metamorphism in the range ~150–400 °C (Rahl *et al.*, 2005; Lahfid *et al.*, 2010; Kouketsu *et al.*, 2014). Therefore, Raman spectroscopy of OM also seems to be a valuable method for the estimation of thermal maturity and maximum temperature. However,

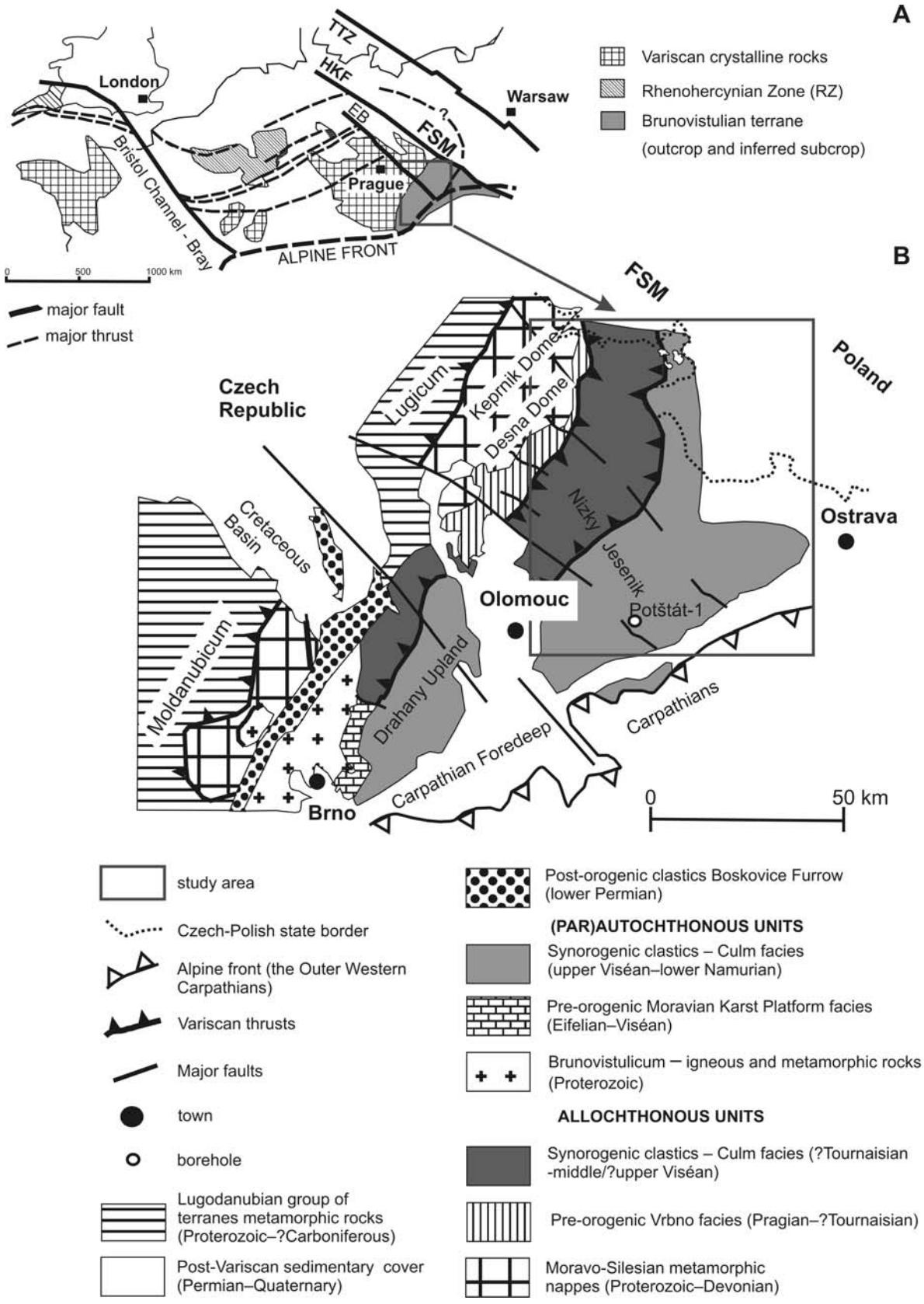

Fig. 1. Location of the area of interest: (A) Geological position of the study area in the European Variscides, (B) Simplified geological sketch map of the Moravo-Silesian Zone (modified after Dvořák, 1994; Kalvoda *et al.*, 2008; Špacek *et al.*, 2015). EB – Elbe Fault, FSM – Fore-Sudetic Monocline, HKF – Hamburg-Kraków Fault, TTZ – Teisseyre-Tornquist Zone.

there are some analytic pitfalls that must be considered, for example, the thermal alteration of OM during measurement, structural defects due to the polishing of graphite, orientation effects, spectral curve-fitting strategies, wavelength-dependent Raman band dispersion, etc. (Wopenka and Pasteris, 1993; Beyssac *et al.*, 2003a, b; Guedes *et al.*, 2010; Hinrichs *et al.*, 2014; Ulyanova *et al.*, 2014; Lünsdorf *et al.*, 2014; Wilkins *et al.*, 2014, 2015; Lünsdorf, 2016).

In this paper, Raman spectroscopy of OM, vitrinite reflectance and fluid inclusion studies are applied to investigate the thermal evolution of the lower Carboniferous Culm facies rocks of the Moravo-Silesian Fold and Thrust Belt (MSFTB; Mazur *et al.*, 2006). This unit is regarded as a part of the Variscan Rhenohercynian belt (e.g., Franke, 1995; Kalvoda *et al.*, 2008), which probably continues across the basement of the Fore-Sudetic Monocline (FSM) in SW Poland (e.g., Franke and Żelaźniewicz, 2000) towards western Europe (Fig. 1). The MSFTB underwent a complex tectonic history, involving crustal shortening, exhumation and probably orogen-parallel extension (Čížek and Tomek, 1991; Schulmann *et al.*, 1991; Dallmeyer *et al.*, 1992; Fritz and Neubauer, 1995; Kumpera and Martinec, 1995; Kalvoda *et al.*, 2008). However, the detailed relationships between tectonics and thermal evolution are poorly understood. Therefore, the aim of the present authors is to better constrain the tectono-thermal evolution of the lower Carboniferous Culm rocks of the MSFTB by examining its OM.

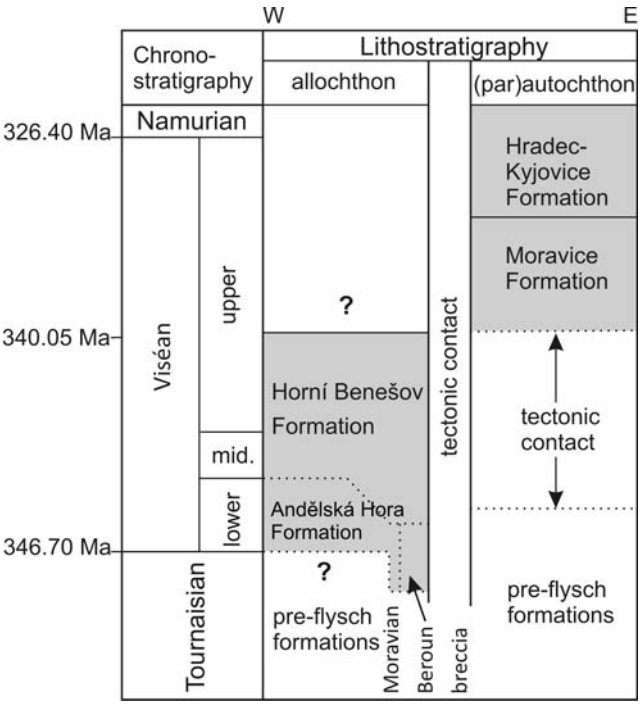

Fig. 2. Generalised stratigraphy of the Culm Basin in the Nízký Jeseník area (modified after Zapletal *et al.*, 1989; Kalvoda *et al.*, 2008; Jirásek *et al.*, 2014).

GEOLOGICAL SETTING

The lower Carboniferous Culm facies of the Nízký Jeseník Mts. in the MSFTB are situated on the NE margin of the Bohemian Massif (Fig. 1). The MSFTB was formed in the eastern part of the Central European Variscides (Unrug, 1966; Dvořák and Paproth, 1969; Unrug and Dembowski, 1971; Schulmann *et al.*, 1991; Franke, 1995; Fritz and Neubauer, 1995; Neubauer and Handler, 1999; Franke and Żelaźniewicz, 2000; Schulmann and Gayer, 2000; Schulmann *et al.*, 2009). The MSFTB corresponds to the eastern part of the Moravo-Silesian Zone (Dallmeyer *et al.*, 1995; Franke and Żelaźniewicz, 2000; Hartley and Ottava, 2001; Mazur *et al.*, 2006). It is composed of unmetamorphosed to slightly metamorphosed Cambrian to upper Carboniferous sediments and volcanics (Kalvoda *et al.*, 2008). Towards the E, the highly deformed MSFTB grades into the less deformed, Moravo-Silesian Culm Basin, which is elongated SW–NE to SSW–NNE, parallel to the overall structural trend in the eastern part of the Bohemian Massif (Fig. 1; Schulmann *et al.*, 1991; Fritz and Neubauer, 1995). The structure of the MSFTB is interpreted as a thin-skinned accretionary wedge, composed of superficial flysch nappes, thrust over the parautochthonous Moravo-Silesian Culm Basin, the Neoproterozoic crystalline basement of the Brunovistulian terrane and its pre-orogenic Devonian sedimentary cover (Dudek, 1980; Kalvoda *et al.*, 2008). The thrusting took place during the late phases of Variscan plate convergence (330–310 Ma; late Carboniferous) under a compressive to right-lateral transpressive tectonic regime (Schulmann and Gayer, 2000). In the Moravo-Silesian Zone, the intensity of deformation, the metamorphism and the sediment composition change in a W–E to NW–SE direction, perpendicular to the Variscan structural grain (Rajlich, 1990; Chadima *et al.*, 2006; Bábek *et al.*, 2005, 2006, 2008). Prominent regional fault systems with NE–SW and NW–SE directions were developed as a result of Variscan tectonics (Rajlich, 1990; Schulmann *et al.*, 1991; Chadima *et al.*, 2006; Kalvoda *et al.*, 2008).

The Culm sediments represent a lower Carboniferous foreland basin that was developed in front of the crystalline nappes of the Moravo-Silesian Zone and partly incorporated into an accretionary wedge as the MSFTB. Deep-water synorogenic siliciclastics of the Culm Basin include conglomerates, greywackes, sandstones, siltstones and mudstones. They were deposited from turbidity currents and sandy and cohesive debris flows. They are exposed in the Drahany and the Nízký Jeseník Culm Sub-basins, separated by the Elbe Fault (Fig. 1) (Kumpera, 1983; Kumpera and Martinec, 1995; Hartley and Otava, 2001; Bábek *et al.*, 2004). Two major tectonic units are distinguished: (1) an allochthonous unit including the Andělská Hora, Horní Benešov, Protivanov and partly Rozstáni formations, and (2) a parautochthonous unit comprising the Moravice, Hradec-Kyjovice, Myslejovice and partly Rozstáni formations (Zapletal *et al.*, 1989; Cháb *et al.*, 1990; Čížek and Tomek, 1991; Grygar and Vavro, 1995; Kumpera and Martinec, 1995; Bábek *et al.*, 2006). The Drahany Sub-basin represented a proximal part and the Nízký Jeseník Sub-basin a distal section of the formerly united Moravo-Silesian Culm Basin (Kumpera and Martinec, 1995; Hartley and Otava, 2001).

The lower Carboniferous Culm sequence is 4.7 to 7.5 km thick (Kumpera, 1983; Kumpera and Martinec, 1995; Hartley and Otava, 2001; Mazur *et al.*, 2006). To the E, the

Culm siliciclastics are overlain by Namurian to Westphalian paralic and continental coal-bearing sediments of the Upper Silesian Coal Basin, representing the final depositional phase in the evolution of the Moravo-Silesian Basin (Kotas *et al.*, 1983; Kalvoda *et al.*, 2008). The age of the synorogenic siliciclastics in the Culm Basin (Fig. 2) is early Viséan to the earliest Namurian (Dvořák, 1973; Kumpera, 1983; Zapletal *et al.*, 1989; Dvořák, 1994; Kalvoda *et al.*, 2008; Jirásek *et al.*, 2014). Lower Carboniferous sediments of the Nízký Jeseník Sub-basin are subdivided into four formations: the Andělská Hora Fm, the Horni Benešov Fm, the Moravice Fm. and the Hradec-Kyjovice Fm (Fig. 2) (Dvořák, 1973, 1994; Kumpera, 1983; Zapletal *et al.*, 1989). The age of these formations is ~346.7 to ~325 Ma (Fig. 2). The recently established age of zircons from the tuffite horizon in Krásné Loučky (340.05 ± 0.22 Ma by TIMS U-Pb) corresponds to the Viséan stage and dates the boundary between the Horní Benešov and Moravice formations (Jirásek *et al.*, 2014).

THERMAL EVOLUTION OF THE MORAVO-SILESIAN FOLD AND THRUST BELT

In the MSFTB, the intensity of deformation and metamorphic alteration generally increases towards the W and NW (Dvořák and Wolf, 1979; Dvořák, 1989; Rajlich, 1990; Franců *et al.*, 1999, 2002; Bábek *et al.*, 2005, 2006, 2008). In the Upper Silesian Coal Basin, which is a foreland of the MSFTB in the Czech Republic and southern Poland, bituminous coals are present (Kotas, 1971; Kotas *et al.*, 1983; Bełka, 1993; Jurczak-Drabek, 1996; Geršlová *et al.*, 2016). The VR_r of the top Carboniferous sediments usually varies from 0.5% in its most eastern part of the Upper Silesian Coal Basin to 1.9% in its western part (Kotas *et al.*, 1983; Jurczak-Drabek, 1996; Kędzior, 2009, 2015). In the Czech part of the Upper Silesian Coal Basin, the values of VR_r are in the range of 0.5–2.3% (Martinec *et al.*, 2005; Sivek *et al.*, 2008; Kandarachevová *et al.*, 2009; Geršlová *et al.*, 2016). The VR_r in the Permian–Miocene overburden is in the range of 0.2–0.5% (e.g., Marynowski *et al.*, 2007; Marynowski and Wyszomirski, 2008; Botor, 2010; Środoń *et al.*, 2014).

In the Moravo-Silesian Culm Basin, most of detailed data come from the Drahany Upland, whilst far fewer data come from the Nízký Jeseník Mts. In the S to SE part of the Drahany Upland, the VR_r ranges from 1.1–2.2%, whereas CAI (Conodont Alteration Index) varies around 3. Towards the W and NW, thermal maturity increases up to 5.2% VR_r and CAI reach 4–5 (Dvořák and Wolf, 1979; Dvořák, 1989; Franců *et al.*, 1999, 2002; Bábek and Franců, 2004; Bábek *et al.*, 2006, 2008). In the Nízký Jeseník Sub-basin, the thermal maturity of OM is high and shows some peculiarities that, so far, have not been fully explained. Dvořák and Wolf (1979) recorded vitrinite R_{max} values in the range of 5.1–9.4%. However, this early study was based partially on measurements on greywackes and many samples that contained reworked organic particles (Dvořák and Wolf, 1979). The most important finding of this work is the SE–NW coalification trend in the Culm Basin. Dvořák (1989) has shown that in the Carboniferous strata in the east (below the Carpathians and the Carpathian Foredeep), the R_{max} values are in the range of 0.5–2.8% and toward the W, they reach 4–6%. Only in four shallow boreholes did the R_{max} reach 8–9%. However, most values in the Andělská Hora Formation are in the range of 4–5 R_{max}%. Illite crystallinity data have shown that most areas of the Culm Basin are in the anchizone (Dvořák, 1989).

In the Drahany Upland, the distribution of vitrinite reflectance and illite crystallinity was interpreted as indicating deep burial with a lower heat flow in the western hinterland and a relatively shallower burial with equal or slightly higher heat flow in the eastern foreland of the basin (Franců *et al.*, 1999, 2002). However, in some wells in the Nízký Jeseník Sub-basin (e.g., Potštát-1), the maturity data do not show any significant depth-related trend. In the Potštát-1 well, a saw-tooth down-hole pattern of R_{min} and R_{max} values indicates that Variscan thrust tectonics did not affect the area before it attained its final thermal maturity (Bábek *et al.*, 2005). This indicates the possible influence of hydrothermal or pressure effects (Bábek *et al.*, 2005). The Mesozoic-Neogene burial did not alter the maturity pattern (Bábek *et al.*, 2005), which is also underlined by low vitrinite reflectance values, both from Culm and molasse Carboniferous strata under the cover of the Carpathians and the Carpathian Foredeep (Dvořák, 1989; Franců *et al.*, 1999). Generally, these data indicate that the rocks of the Culm basin attained their maximum thermal maturity during the final stages of the thrust-related Variscan deformation, in the late Carboniferous to early Permian Period.

Numerous, well-known hydrothermal veins, occurring in the Nízký Jeseník Mts., are a record of fluid influence on the Culm rocks. These polymetallic veins are concentrated in historical mining districts, where mainly silver and lead and also gold were mined (Fojt and Vecera, 2000; Kučera and Slobodnik, 2002; Zimák *et al.*, 2002; Kučera *et al.*, 2010; Dolníček *et al.*, 2014; Janiková *et al.*, 2015). Common ore minerals are galena, sphalerite, chalcopyrite, pyrite and marcasite, whilst quartz, Mg, Fe-carbonates, calcite and barite represent gangue minerals. The veins have mostly massive, brecciated, deformational and drusy structures and their thickness ranges between a few millimetres and half a metre (Zimák *et al.*, 2002; Kučera and Slobodnik, 2002; Dolníćek *et al.*, 2014). The age of vein formation is uncertain. Kučera and Slobodník (2002) argued that these veins fill extensional structures oriented perpendicularly to the bedding planes and their origin is post-Variscan and possibly related to Alpine brittle strain. The regional distribution of hydrothermal mineralisation points to a more extensive migration of fluids along fractures, formed owing to a regional stress field, perhaps developed by the movement of large crustal blocks during one of the phases of Alpine (Kučera and Slobodník (2002) or late to post-Variscan (Kříbek *et al.*, 2009) deformation.

In summary, there is a general trend of strain and thermal overprint from late diagenesis in the distal foreland in the SE to very low-grade metamorphism in the westernmost part. The Palaeozoic sediments underwent metamorphism during the late Variscan peak metamorphism, which was probably reached just after the folding (Dvořák *et al.*, 1997).

Table 1

List of samples and vitrinite reflectance data

Sample	Coordinates		Lithology	R_{min}	R_{min} mean	SD	N	R_{max}	R_{max} mean	SD	N	R_r mean	SD	N	Temperature T_b (°C)	Temperature T_h (°C)
BR	50°0′5.57″N	17°29′24.47″E	mudstone	n.d.	n.d.	n.d.	n.d.	n.d.	n.d.	n.d.	n.d.	2.11*	0.32	15	205	262
Bu	49°52′2.42″N	18°0′6.90″E	claystone	n.d.	n.d.	n.d.	n.d.	n.d.	n.d.	n.d.	n.d.	2.81*	0.41	50	219	284
CZ19	49°47′43.92″N	17°33′31.52″E	mudstone	0.71	1.74	0.72	30	3.82	2.21	0.92	30	2.32	0.42	50	203	260
CZ26	49°58′53.15″N	17°29′55.03″E	claystone	1.86	2.69	0.46	25	3.89	3.25	0.34	25	2.81	0.45	50	219	284
CZ30	50°10′56.69″N	17°31′18.74″E	claystone	n.d.	n.d.	n.d.	n.d.	n.d.	n.d.	n.d.	n.d.	2.78*	0.39	55	218	283
CZ39	49°45′22.43″N	17°55′24.59″E	mudstone	1.15	1.46	0.23	6	1.77	1.70	0.08	6	3.67	0.19	50	240	318
CZ4	49°36′17.28″N	17°41′15.84″E	claystone	n.d.	n.d.	n.d.	n.d.	n.d.	n.d.	n.d.	n.d.	3.03*	0.50	90	225	294
CZ51	49°48′39.76″N	17°16′25.68″E	metapelite	2.41	3.49	0.51	50	4.84	3.94	0.59	50	3.73	0.56	25	242	321
CZ6	50°1′35.27″N	17°44′19.58″E	mudstone	n.d.	n.d.	n.d.	n.d.	n.d.	n.d.	n.d.	n.d.	3.05*	0.50	75	225	295
CZ66	50°2′24.58″N	17°22′45.09″E	metapelit	n.d.	n.d.	n.d.	n.d.	n.d.	n.d.	n.d.	n.d.	2.63	0.34	50	213	276
CZ74	49°47′30.13″N	17°45′51.06″E	claystone	n.d.	n.d.	n.d.	n.d.	n.d.	n.d.	n.d.	n.d.	2.75	0.27	15	217	282
CZ78	49°55′11.79?N	17°21′38.21?E	mudstone	n.d.	n.d.	n.d.	n.d.	n.d.	n.d.	n.d.	n.d.	2.45*	0.49	65	208	267
CZ9	49°45′54.10″N	17°41′5.17″E	claystone	n.d.	n.d.	n.d.	n.d.	n.d.	n.d.	n.d.	n.d.	2.65*	0.34	61	214	277
DVO	49°50′12.78″N	17°30′37.68″E	claystone	2.06	2.53	0.28	20	3.44	3.06	0.23	20	2.81	0.44	20	219	284
HOZ	49°46′17.59″N	17°19′31.10″E	metapelite	1.65	2.23	0.48	25	3.59	2.61	0.52	25	2.89	0.45	25	221	288
KRL	50°7′13.25″N	17°37′22.89″E	mudstone	n.d.	n.d.	n.d.	n.d.	n.d.	n.d.	n.d.	n.d.	2.81	0.49	10	219	284
KUN	50°2′51.96″N	17°30′4.56″E	mudstone	1.96	2.44	0.26	24	3.53	2.91	0.25	24	2.97	0.29	50	223	291
POK2	50°16′47.11″N	17°26′49.85″E	phyllite	n.d.	n.d.	n.d.	n.d.	n.d.	n.d.	n.d.	n.d.	4.42*	0.62	10	255	342
SOS	50°0′35.43″N	17°38′18.83″E	mudstone	1.67	2.30	0.31	20	2.97	2.54	0.26	20	3.00	0.40	20	224	293
SV	49°46′16.35″N	17°58′58.22″E	mudstone	2.62	3.42	0.24	70	4.00	3.67	0.15	70	3.55	0.14	60	238	314
TES	49°44′16.76″N	17°21′57.09″E	metapelite	1.60	2.89	0.62	32	4.12	3.37	0.58	32	2.93	0.50	25	222	290
ZLH	50°14′23.62″N	17°26′9.28″E	phyllite	n.d.	n.d.	n.d.	n.d.	n.d.	n.d.	n.d.	n.d.	3.90*	0.40	50	245	326

Analyst I. Jelonek. except for samples with * measured by D. Botor; R_r, R_{min}, R_{max} – values given in (%); SD – standard deviation; N – number of measurements; n.d. – no data; T_b (°C) – maximum temperature calculated from R_r data for burial model (Barker and Pawlewicz, 1994); Th (°C) – maximum temperature calculated from Rr data for hydrothermal model (Barker and Pawlewicz, 1994)

MATERIALS AND METHODS

A total of 22 fine-grained rock samples was collected from lower Carboniferous outcrops in the Nízký Jeseník Mts. (Tab. 1). Samples were taken from a depth of 0.3–0.5 m to avoid the influence of weathering. Four samples of quartz and calcite were also collected from small veins cutting the greywackes.

Vitrinite reflectance

The rock samples were cut perpendicular to the bedding and from these rock pieces polished slides were prepared for vitrinite reflectance measurements (R_{max}, R_{min} and VR_r). Vitrinite reflectance was measured to determine the thermal maturity of the samples. Vitrinite reflectance measurements were performed using a Zeiss Axio Imager 2mM microscope for incident light, a 50×/0.85 Epiplan-Neofluar oil immersion objective and a 546 nm filter, Zeiss immersion oil n_e = 1.518, at a temperature of 23 °C. Mineral standards of known reflectance were used for calibration: sapphire (0.590%), yttrium-aluminium garnet (0.901%), gadolinium-gallium garnet (1.718%), cubic zirconium (3.130%) and strontium-titanate (5.39%). The applied microscopical investigations closely followed the guidelines published by Taylor *et al.* (1998), Pusz *et al.* (2014) and Hackley *et al.* (2015). VR_r was used as an input parameter for the estimation of maximum palaeotemperature after Barker and Pawlewicz (1994). In the present study, the formula Temperature1 = (lnRr + 1.68)/0.0124 for the burial heating model and Temperature2 = (lnRr + 1.19)/0.00782 for the hydrothermal heating model after Barker and Pawlewicz (1994) was used. The formulas are calibrated up to 7% VR_r (Barker and Pawlewicz, 1994).

Raman spectroscopy

Type of samples

Raman measurements were performed on slides of polished rock but, for comparison, one thin-section also was used. According to Aoya *et al.* (2010), both types of samples can be used, which also was suggested earlier by Beyssac *et al.* (2003a) and Rahl *et al.* (2005) in the case of highly disordered low-grade OM. However, in higher-ordered OM (particularly in graphite) several authors showed that the polishing of a sample could cause a change in the Raman record (Katagiri *et al.*, 1988; Wopenka and Pasteris, 1993). Beyssac *et al.* (2003a) showed that in poorly organ-

ised OM (R2 higher than 0.5), there is no significant difference, whereas in well-organised OM (R2 lower than 0.5) the spectra measured at the surface exhibit a higher contribution of the defect bands (D1 and D2). According to Aoya *et al.* (2010), even in the R2 range 0.1–0.3 Raman results from both thin sections and polished slabs (chips) are comparable. Also according to Lünsdorf (2016), in the VR_r measuring range of 1 to 7%, the Raman spectra are unaffected by polishing, if no final polishing below 1 μm is used. Therefore, no polishing less than 1μm was used in this study. In a final step, only 1 μm monocrystalline diamond slurry was used. Further discussion of sample preparation is given in Lünsdorf (2016). All the samples in the present study have R2 values higher than 0.5 and their spectra show that they consist of poorly organised OM. Therefore, rock slides were used.

Measurements

Raman spectra were obtained using a Thermo Scientific^{TM} DXR^{TM} with a 532 nm Nd-YAG laser passed through a confocal microscope (Olympus, BX51: Olympus, Tokyo, Japan) with the 100×, 50× and 10× objectives. The laser power on the sample surface was set at 1–2 mW. The scattered light was collected by backscattered geometry with a 25 μm pinhole and a holographic notch filter and finally dispersed using a 900 lines/mm grating and analysed by a cooled CCD detector of 256 × 1024 pixels. Spatial resolution was about 1 μm and wave number resolution about 1 cm^{-1}. The acquisition time was 30 s (assumed as a minimum time to obtain reliable results: Kouketsu *et al.*, 2014). The Raman system was calibrated against the 520.4 cm^{-1} line of a Si-wafer. In each sample, 6–27 different organic particles (usually 25 as suggested by Aoya *et al.*, 2010) were measured.

Raman spectra

The Raman spectrum of OM is composed of first-order (1000–1800 cm^{-1}) and second-order (2500–3100 cm^{-1}) regions (e.g., Nemanich and Solin, 1979; Pasteris and Wopenka, 1991; Beyssac *et al.*, 2002a). Here we focus on the first-order range as the most important (Beyssac *et al.*, 2002a, 2003a, 2003b). There are at least five Raman bands in the first-order spectrum of OM (~1000–2000 cm^{-1}) visible, particularly in the low-grade metamorphic range (Lünsdorf *et al.*, 2014). These bands are denominated as D1 (~1350 cm^{-1}), D2 (~1620 cm^{-1}), D3 (~1500 cm^{-1}), D4 (~1250 cm^{-1}) and G (~1580 cm^{-1}). The G band is assigned to the Raman active E2g optical phonon in graphite (Tuinstra and Koenig, 1970; Reich and Thomsen, 2004). The D1 and D2 bands are defect-induced (Pócsik *et al.*, 1998; Matthews *et al.*, 1999; Pimenta *et al.*, 2007) and depend on the excitation energy due to double-resonant Raman scattering (Reich and Thomsen, 2004). The D3 band supposedly originates from amorphous carbons and the D4 band is attributed to sp2–sp3 bonds or C–C and C=C stretching vibrations of polyene-like structures (Sadezky *et al.*, 2005 and references therein). The band assignments are discussed by Tuinstra and Koenig (1970), Beny-Bassez and Rouzaud (1985), Reich and Thomsen (2004), Beyssac *et al.* (2003a, b), Sadezky *et al.* (2005), Ulyanova *et al.* (2014) and also summarised by Potgieter-Vermaak *et al.* (2011) and Kouketsu *et al.* (2014). The methodology for peak decomposition of the Raman spectra of OM is not fully established (see Lünsdorf *et al.*, 2014). Despite many studies on the topic (e.g., Tuinstra and Koenig, 1970; Ferrari and Robertson, 2000; Beyssac *et al.*, 2003a, b), there is not yet a clear consensus on the best way to treat OM Raman bands, especially for low-grade OM. This difficulty reflects the complexity of OM structure in the low metamorphic or diagenetic range. There are several fitting procedures available for such a disordered OM, for example, a four-band fitting using a Voigt profile (Beyssac *et al.*, 2002a, a; Rahl *et al.*, 2005), or a five-band combination of Lorentzian and Gaussian profiles (Sadezky *et al.*, 2005).

The present study focuses on the first-order region, which is associated with up to five discriminative bands of OM. The Raman spectra were decomposed, using Omnic ver. 4.12 software (Thermo Fisher Scientific, Inc.) with a pseudo-Voigt function (Gaussian-Lorentzian Sum) and corrected for the fluorescence background by subtracting a linear baseline in the spectral range 1000–1800 cm ^{1}. The workflow of Kouketsu *et al.* (2014) and the methodological aspects of decomposition of the Raman spectra of OM highlighted by Aoya *et al.* (2010) and Lünsdorf *et al.* (2014) were taken into account. Generally, the line shape of the Raman spectrum varies with increasing order of the OM, which increases with the degree of metamorphism (e.g., Wopenka and Pasteris, 1993; Beyssac *et al.*, 2002b; Morga, 2011, 2014). The number of Raman bands decreases from low to high metamorphic conditions (Wopenka and Pasteris, 1993; Beyssac *et al.*, 2002b). Poorly ordered OM contains two additional bands D3 (~1510 cm^{-1}) and D4 (~1245 cm^{-1}) (e.g., Rahl *et al.*, 2005; Kouketsu *et al.*, 2014). The G and D2 bands are not separated and they form one band (G_L) around 1600 cm^{-1} and the D1 band is very wide (e.g., Rahl *et al.*, 2005; Lahfid *et al.*, 2010; Kouketsu *et al.*, 2014; Lünsdorf *et al.*, 2014). The intensity of the G_L band is higher than that of the D1 band. With an increase of OM order, the G and D2 bands become distinguishable. The D3 and D4 bands disappear gradually with an increase in temperature, while the D1 band becomes narrower. In the temperature range ~300–400 °C (Kouketsu *et al.*, 2014), the intensity of the D1 band becomes higher than that of the G and D2 (G_L) bands. Above this range, the intensity of the D1 band again becomes lower and narrower (see also Kouketsu *et al.*, 2014). Further heating results in the disappearance of the D1 and D2 bands. In pure graphite, only the G band occurs (Tuinstra and Koenig, 1970; Beyssac *et al.*, 2002a; Kouketsu *et al.*, 2004). Although the width of the G band seems to be a significant structural parameter for tracing both coalification and graphitisation of OM, Rantitsch *et al.* (2016) and also Rodrigues *et al.* (2013) showed a limited sensitivity of Raman parameters, when they are correlated with VR_r.

Temperature estimation

Various Raman ratios that correlate with the maximum metamorphic temperature can be calculated (Beyssac *et al.*, 2002a; Rantitsch *et al.*, 2004; Rahl *et al.*, 2005; Aoya *et al.*, 2010; Lahfid *et al.*, 2010; Kouketsu *et al.*, 2014; Lünsdorf

and Lünsdorf, 2016). The most common are the R1 (intensity ratio, D1 G) and R2 (area ratio, D1 [G + D1 + D2]) (Beyssac *et al.*, 2002a) and the RA1 = (D1 + D4) (D1 + D2 + D3 + D4 + G) area ratio and RA2 = (D1 + D4) (D2 + D3 + G) area ratio (Lahfid *et al.*, 2010).

A linear correlation between the R2 ratio and temperature is observed in the range of 330–650 °C. At temperatures lower than 330 °C, the R2 parameter is nearly constant around 0.7 (Beyssac *et al.*, 2002a). In poorly organised OM, R2 characterisation is not appropriate, because the extension of the coherent domains constituted by the aromatic rings is too small. At temperatures higher than 650 °C, OM shows a triperiodic structure and the R2 ratio remains at a constant value (< 0.05), thereby setting the upper limit to its use (Beyssac *et al.*, 2002a). In contrast, the R2 ratio *versus* pressure shows no clear trend (Beyssac *et al.*, 2002a). However, Barzoi (2015) recently showed that pressure could also cause slight changes of Raman spectra. Rahl *et al.* (2005) used both the R1 and R2, which seems to be less precise for temperatures below 330 °C in the low-grade metamorphism zone. Lahfid *et al.* (2010) proposed a Raman OM geothermometer, applicable in a range of ~200–320 °C; however, it is disputable whether the proposed peak-fitting method is applicable to temperatures below 200 °C and higher than 320 °C. Lahfid *et al.* (2010) constructed a method for one metamorphic region only (the Glarus Unit in the Alps) and, as stated by the authors, it is unclear how far this method can be accurately applied to other areas. Recently, Kouketsu *et al.* (2014) proposed a fitting procedure applicable over a wide range of temperatures, in which estimates are associated with relatively small errors in a temperature calibration range (150–400 °C) that is suitable for the study area.

Fluid inclusions

Fluid inclusions were analysed in quartz and calcite samples taken from veins. The microthermometric measurements were carried out on groups of inclusions that show a constant vapour-to-liquid ratio (Roedder, 1984; Goldstein and Reynolds, 1994). Careful attention was paid to changes of the inclusion shape to avoid the measurement of re-equilibrated inclusions. Double polished sections about 200 μm thick were used. The measurements were carried out using a Linkam THMSG600 heating and freezing stage, mounted on a NIKON ECLIPSE E600 microscope with 20×, 50× and 100× objectives. The stage was calibrated using pure H_2O-CO_2 synthetic inclusions (Tm = –56.9 °C) and the known homogenisation temperature of pure H_2O inclusions (of critical density of Tm_{ice} = 0.0 °C, Th = 374 °C). The heating-freezing rate of 5 °C/min was applied with an accuracy of 0.1 °C.

RESULTS

Vitrinite reflectance

The samples analysed contain several types of dispersed OM that differ in morphology, reflectance and texture (Fig. 3). The size of the maceral fragments varies from less than 5 to more than 100 μm. The shape of phytoclasts is irregular, sometimes subspherical in vitrodetrinite and highly variable in inertodetrinite. Generally, vitrinite is characterised by textureless surfaces and a strong optical anisotropy. Care was taken to obtain non-weathered samples in order to avoid any influence of weathering on vitrinite reflectance. Typical features of weathered vitrinite are discussed in Taylor *et al.* (1998: p. 529; see references therein), but were not observed in the sample set of the present study. R_{max} varies from 1.77% to 4.84% and R_{min} is from 0.71% to 2.62% (Tab. 1). Mean VR_r values range from 2.11 to 4.42 (Table 1; Fig. 4), with standard deviation of 0.14–0.62 and number of measured organic particles ranging from 15 to 90 (usually 50–75; Table 1). The VR_r values were transformed into maximum palaeotemperatures using the Barker and Pawlewicz (1994) method. Maximum palaeotemperatures were calculated for the regional burial model (T_b; Barker and Pawlewicz, 1994) in the range 203–255 °C, whilst maximum palaeotemperatures were calculated for the hydrothermal model (T_h, Barker and Pawlewicz, 1994) in the range 260–342 °C (Tab. 1; Fig. 4). The calculated palaeotemperatures increase toward the W and NW (Fig. 4); however, an overall trend of increasing thermal maturity from E to W and NW is faintly visible (Fig. 4). Generally, this can be interpreted as a result of similar palaeothermal exposure of the rocks in the entire area; although the scatter of the vitrinite reflectance data could be partially due to an intensive folding and faulting of the strata leading to many small-scale anticlines and synclines. Bruns and Littke (2015) showed that a partially significant scatter of measured vitrinite reflectance could be observed, not only due to the high rank and associated anisotropic character, but also due to lithological dependency (sandstone *vs*. shale *vs*. coal). At very high levels of thermal maturity, vitrinite reflectance depends not only on maximum palaeotemperature but also on lithology, which leads to differences in pressure propagation (Bruns and Littke, 2015). However, all of the samples come from fine-grained rocks (Tab. 1) and no vitrinite reflectance measurements were performed in other lithologies. Cleavage, which is often visible in the Culm rocks, can also cause some scatter of vitrinite reflectance (Littke *et al.*, 2012) but this feature can only be significant in the samples located in the westernmost area of the Andělská Hora Formation The thermal maturity of all samples analysed reaches the anthracite and partly in some grains the meta-anthracite stage of organic metamorphism (Taylor *et al.*, 1998; Kwiecińska and Petersen, 2004). The measured vitrinite reflectance data correlate with the Nowak's (2003) data from the northern part of the study area and the Bábek *et al.* (2008) data from the southern part. However, the VR_{max} values of Dvořák and Wolf (1979) and Dvořák (1989) cannot be converted into VR_r because R_{min} is not given in their works. Generally, their R_{max} values are higher than the VR_r, calculated here, as might be expected (see Taylor *et al.*, 1998). Very high levels of thermal maturity (above ~2.0% VR_r) also were confirmed by the palynological investigation of several samples (P. Filipiak, pers. comm., 2015).

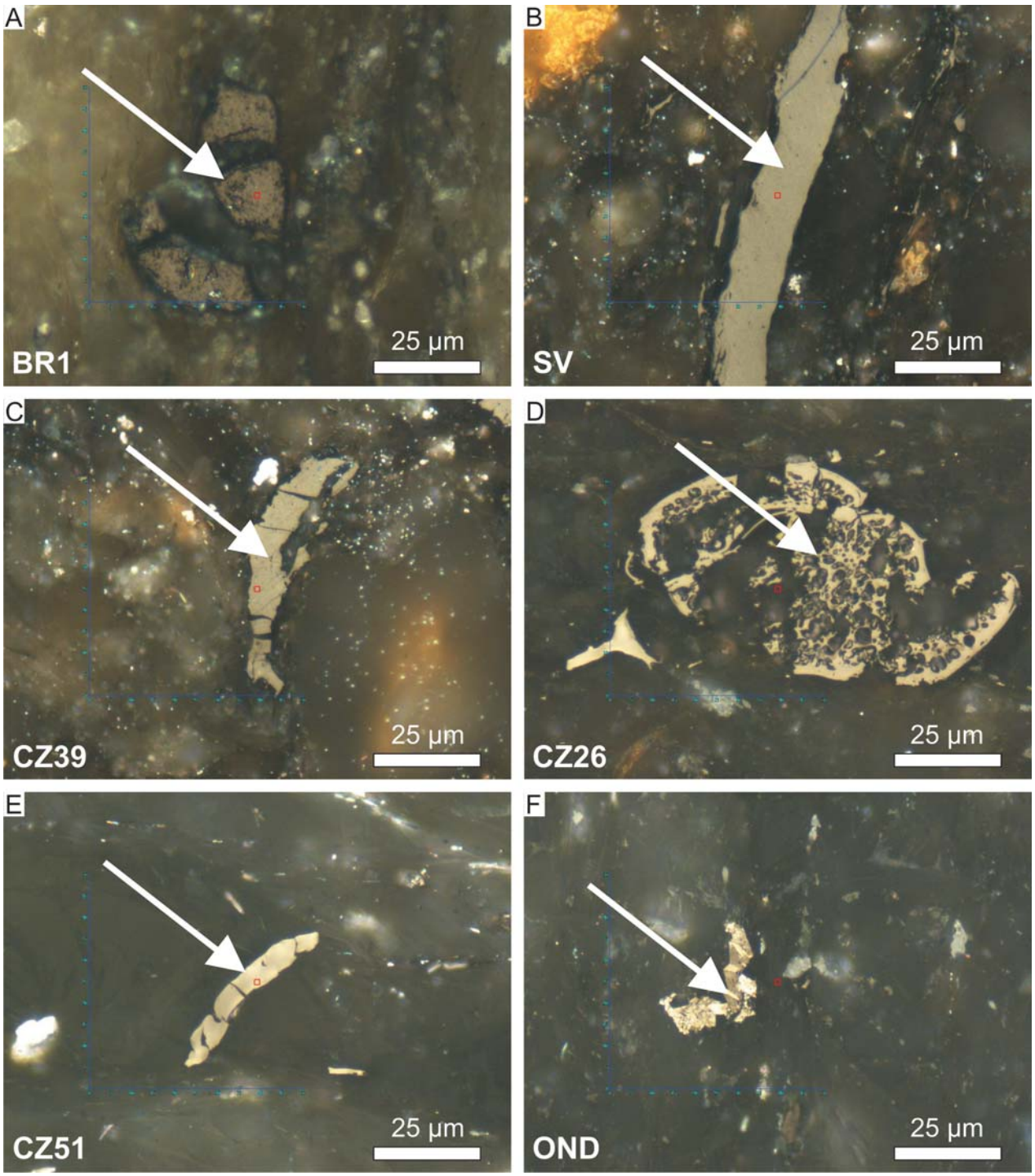

Fig. 3. Microphotography of organic matter from the Culm Basin. Scale bar = 25 µm. **A–C.** Vitrinite. **D.** Funginite. **E–F.** Transitional material (see Diesel *et al.*, 1978). The D–F organic particles were excluded from the samples subject to temperature estimation.

Raman spectroscopy

Raman spectroscopy data of OM from the Culm Basin are presented in Table 2 and Figures 5 to 8. Representative Raman spectra are shown in Figure 5. The Raman data (Tab. 2; Fig. 5) reflect the continuous ordering of OM by a progressive thermal overprint. With rising temperature, the position of the D1 and D2 peaks shift to higher values, the position of G shifts to lower Raman values and the full width at half maximum (FWHM) values becomes lower (Tab. 2; Fig. 5). The D1 band position varies from 1332.2 to 1356.1 cm^{-1} and increases with metamorphic temperatures. The G band range is 1583.6–1593.9 cm^{-1}, while the D2 band range is 1604–1618.6 cm^{-1} and the D3 band is 1469.7–1537.0 cm^{-1} (Tab. 2). FWHM-D1 allows two groups of samples to be distinguished: POK2, ZLH and then all other sam-

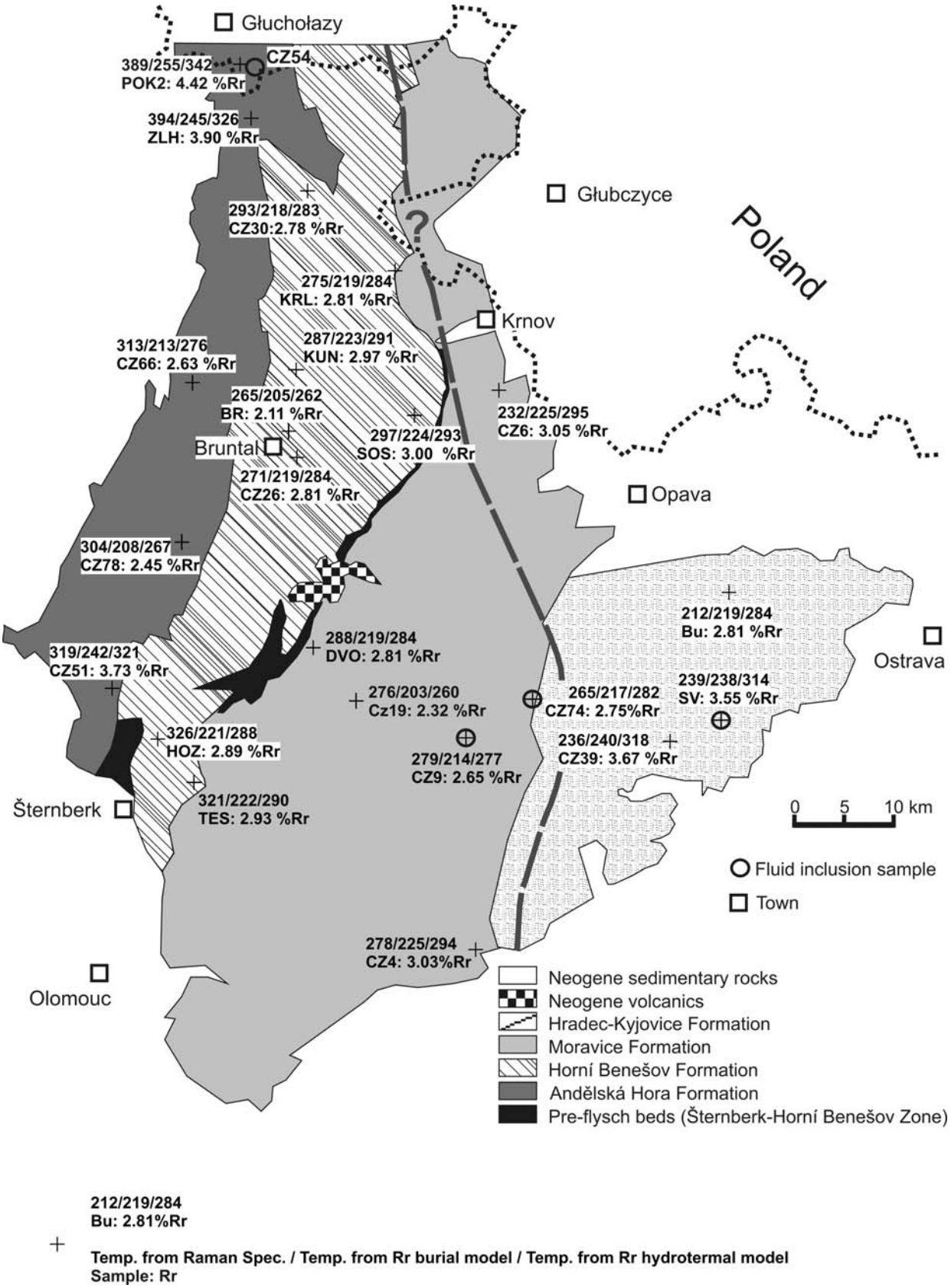

Fig. 4. Distribution of maximum palaeotemperatures in the Culm Basin derived from vitrinite reflectance and from Raman spectroscopy (geological map modified after Unrug, 1977; Kościówko, 1982; Dvořák, 1994; Pouba, 1996; Roth, 1996; Kalvoda *et al.*, 2008). Dashed line represents estimated extent of significant fluid migration.

Table 2

Raman spectroscopy data

Sample	Centre					Height					FWHH					Area				
	D4	D1	D3	G	D2	D4	D1	D3	G	D2	D4	D1	D3	G	D2	D4	D1	D3	G	D2
Bu (n = 27)																				
Average	1245.0	1332.3	1529.5	1593.0	1605.6	171.4	852.3	81.9	1015.7	341.1	143.1	123.8	112.3	44.0	23.2	30746.2	196638.5	10194.8	70058.6	8952.2
Median	1245.0	1332.5	1529.8	1593.0	1605.6	172.9	874.7	84.5	1079.1	275.7	142.5	124.1	111.0	43.7	22.9	31626.5	205040.8	10659.0	73105.5	7497.8
SD	0.0	1.5	5.8	0.0	0.6	40.6	153.3	12.7	185.1	174.9	9.0	9.5	4.0	2.1	2.8	7564.3	35909.0	1853.1	12779.9	6093.0
Co.V. [%]	0.0	0.1	0.4	0.0	0.0	23.7	18.0	15.4	18.2	51.3	6.3	7.7	3.6	4.8	11.9	24.6	18.3	18.2	18.2	68.1
SV (n = 28)																				
Average	1245.0	1335.9	1490.6	1593.0	1605.8	264.1	637.5	142.7	910.4	247.6	176.2	111.4	174.3	46.7	19.5	58767.4	109175.0	26831.3	67484.5	6518.5
Median	1245.0	1335.8	1491.5	1593.0	1605.6	274.3	641.4	141.7	977.1	160.9	176.8	110.7	175.1	46.1	18.8	59072.2	103975.5	27083.0	68323.1	3198.6
SD	0.0	2.0	5.9	0.0	0.8	58.1	123.0	25.8	253.2	237.7	10.8	4.9	7.2	3.1	4.6	13591.3	20662.9	5232.8	14774.7	10127.5
Co.V. [%]	0.0	0.1	0.4	0.0	0.1	22.0	19.3	18.1	27.8	96.0	6.1	4.4	4.1	6.7	23.3	23.1	18.9	19.5	21.9	155.4
CZ39 (n = 25)																				
Average	1245.0	1335.6	1488.8	1593.0	1605.4	279.1	791.4	161.5	1010.3	344.4	169.5	112.4	183.3	49.4	23.8	56467.7	139314.5	31662.1	78002.3	9595.8
Median	1245.0	1335.5	1486.4	1593.0	1605.3	269.4	765.9	162.2	983.7	279.4	170.0	113.2	188.9	49.4	23.8	56072.9	133184.7	31665.0	76437.1	7324.6
SD	0.0	2.0	10.9	0.0	0.6	53.2	128.0	20.4	143.3	151.2	7.2	5.9	12.1	3.4	2.5	10012.2	20739.4	5165.7	10429.2	5172.3
Co.V. [%]	0.0	0.1	0.7	0.0	0.0	19.1	16.2	12.6	14.2	43.9	4.3	5.3	6.6	6.9	10.6	17.7	14.9	16.3	13.4	53.9
CZ74 (n = 25)																				
Average	1245.0	1332.2	1527.1	1593.0	1606.4	166.6	859.5	129.9	660.5	579.8	242.3	99.0	159.5	46.7	30.3	58978.5	136296.6	39451.3	47714.6	18912.3
Median	1245.0	1332.3	1523.2	1593.0	1606.6	165.9	879.0	114.0	668.7	559.7	236.0	99.5	135.9	47.1	30.5	56450.2	138290.8	20001.7	49012.1	18456.6
SD	0.0	1.2	8.8	0.0	1.3	46.6	84.5	39.2	135.5	93.4	32.0	4.3	48.9	4.6	1.8	31791.8	13805.9	31931.8	6972.1	4035.1
Co.V. [%]	0.0	0.1	0.6	0.0	0.1	28.0	9.8	30.2	20.5	16.1	13.2	4.3	30.6	9.8	5.9	53.9	10.1	80.9	14.6	21.3
CZ74_thin-sec (n = 18)																				
Average	1245.0	1333.4	1530.3	1593.0	1607.8	142.5	567.1	98.8	467.9	377.4	270.6	95.2	220.8	44.2	29.4	62697.7	83053.0	43490.2	31803.0	11811.5
Median	1245.0	1332.7	1533.5	1593.0	1607.7	140.2	564.1	100.7	476.3	365.8	275.3	95.7	223.8	43.0	29.4	62026.6	83719.7	46391.5	31608.3	11309.3
SD	0.0	2.0	9.3	0.0	0.4	29.4	113.4	20.7	132.3	57.0	10.1	1.8	9.2	3.9	1.6	13294.1	17704.1	12160.7	7495.2	1789.5
Co.V. [%]	0.0	0.1	0.6	0.0	0.0	20.6	20.0	20.9	28.3	15.1	3.7	1.9	4.2	8.8	5.3	21.2	21.3	28.0	23.6	15.2
CZ6 (n = 25)																				
Average	1245.0	1332.3	1523.3	1593.0	1606.4	110.6	932.8	97.7	825.1	505.5	192.1	114.3	97.2	48.3	28.4	23716.0	187241.3	10160.1	61981.1	15443.7
Median	1245.0	1331.8	1522.8	1593.0	1606.4	126.3	957.0	101.6	881.5	541.8	192.5	113.1	96.3	47.5	28.4	26407.6	190916.5	10617.6	67209.1	15851.8
SD	0.0	1.5	3.1	0.0	0.9	35.0	184.3	17.6	185.7	168.9	4.5	5.6	2.9	3.2	2.0	7426.5	31624.0	1897.1	12435.2	5567.9
Co.V. [%]	0.0	0.1	0.2	0.0	0.1	31.7	19.8	18.0	22.5	33.4	2.4	4.9	3.0	6.6	6.9	31.3	16.9	18.7	20.1	36.1
CZ9 (n = 25)																				
Average	1245.0	1333.2	1513.8	1593.0	1606.8	181.0	841.6	115.4	677.4	554.9	231.3	92.7	151.7	44.2	29.6	52583.3	114418.6	21542.7	46709.7	17922.0
Median	1245.0	1333.1	1513.5	1593.0	1606.7	182.0	832.0	112.5	676.2	557.7	229.3	92.1	159.4	43.9	29.6	46664.4	110733.6	22198.5	46397.4	18019.7
SD	0.0	1.1	2.7	0.0	0.5	29.3	87.4	12.4	95.3	75.0	17.2	2.1	18.9	2.9	1.1	19867.8	13819.1	3979.2	4929.4	2849.4
Co.V. [%]	0.0	0.1	0.2	0.0	0.0	16.2	10.4	10.8	14.1	13.5	7.4	2.3	12.4	6.5	3.8	37.8	12.1	18.5	10.6	15.9
CZ4 (n = 25)																				
Average	1245.0	1334.2	1520.1	1593.0	1607.2	158.4	912.5	112.2	605.1	718.2	154.3	92.9	122.4	40.7	29.9	35955.1	131551.0	21426.1	38122.8	29029.6
Median	1245.0	1334.1	1517.4	1593.0	1607.6	170.7	927.9	113.4	627.1	725.2	154.3	92.6	122.8	38.7	29.4	41239.0	133251.0	20728.7	39076.6	27927.7
SD	0.0	0.7	5.5	0.0	1.4	27.4	68.7	11.3	106.8	117.8	0.0	2.2	18.2	5.4	2.0	10392.9	8750.1	5711.1	5337.8	6925.9
Co.V. [%]	0.0	0.1	0.4	0.0	0.1	17.3	7.5	10.1	17.7	16.4	0.0	2.4	14.9	13.4	6.6	28.9	6.7	26.7	14.0	23.9
CZ19 (n = 25)																				
Average	1245.0	1338.3	1517.7	1593.0	1608.6	109.8	600.3	80.8	452.9	305.3	245.7	94.1	144.5	46.6	31.4	34167.3	81079.4	13870.5	32903.4	10253.8
Median	1245.0	1338.2	1517.7	1593.0	1608.5	111.8	616.4	80.9	458.1	305.4	244.1	93.9	148.2	46.3	31.4	34438.8	82012.6	12977.9	33598.7	10148.7
SD	0.0	0.6	1.6	0.0	0.7	17.0	60.3	9.9	62.2	43.3	6.9	1.6	11.0	2.3	1.3	6805.3	7142.8	3696.7	3267.4	1604.7
Co.V. [%]	0.0	0.0	0.1	0.0	0.0	15.4	10.0	12.3	13.7	14.2	2.8	1.7	7.6	4.9	4.2	19.9	8.8	26.7	9.9	15.7

SD – standard deviation; Co.V. – coefficient of variation = (SD/average) × 100; n.m. – not measured

Sample	Centre					Height					FWHH					Area				
	D4	D1	D3	G	D2	D4	D1	D3	G	D2	D4	D1	D3	G	D2	D4	D1	D3	G	D2
DVO (n = 22)																				
Average	1245.0	1342.3	1510.9	1592.4	1610.1	67.4	378.6	50.4	232.0	229.1	201.0	88.4	170.2	47.4	33.3	14889.0	46311.4	10093.9	17384.2	8241.4
Median	1245.0	1340.9	1510.3	1593.0	1609.4	76.1	406.6	58.2	258.0	250.1	201.9	91.6	170.3	48.0	33.4	16877.9	51018.9	10808.5	19391.1	8911.7
SD	0.0	3.2	6.8	2.0	2.6	23.5	99.5	17.8	68.0	72.4	5.7	12.7	4.0	6.0	2.7	5165.0	13332.6	3972.0	5440.0	2554.2
Co.V. [%]	0.0	0.2	0.5	0.1	0.2	34.9	26.3	35.3	29.3	31.6	2.8	14.3	2.3	12.7	8.2	34.7	28.8	39.4	31.3	31.0
KRL (n = 25)																				
Average	1245.0	1332.4	1513.4	1593.0	1605.1	63.2	339.1	33.8	206.3	355.7	174.2	94.3	94.8	55.0	29.5	13128.6	57254.4	4693.0	17757.8	11462.5
Median	1245.0	1332.5	1513.0	1593.0	1605.0	63.5	348.1	34.3	204.4	371.2	171.2	94.4	89.7	55.5	29.2	12049.1	57551.1	4392.5	17851.7	11879.1
SD	0.0	0.9	2.8	0.0	0.5	17.8	68.5	6.5	40.2	87.4	9.6	4.6	10.9	1.8	0.6	4627.7	10553.9	1280.2	3431.1	2754.5
Co.V. [%]	0.0	0.1	0.2	0.0	0.0	28.2	20.2	19.2	19.5	24.6	5.5	4.9	11.5	3.3	1.9	35.2	18.4	27.3	19.3	24.0
KUN (n = 25)																				
Average	1245.0	1341.5	1511.4	1593.0	1608.7	46.4	255.9	31.7	144.1	162.8	199.0	88.8	171.1	50.7	34.3	10585.5	30494.6	6261.4	11376.2	5952.9
Median	1245.0	1341.6	1513.3	1593.0	1608.8	46.7	258.4	32.1	144.2	165.6	199.1	88.9	169.7	49.5	34.4	9982.4	30329.3	6293.2	11367.9	6093.9
O.S.	0.0	0.6	5.2	0.0	0.6	3.9	18.3	2.6	17.8	15.1	5.3	1.7	4.0	4.0	0.9	2168.9	2053.3	591.1	852.4	655.8
Co.V. [%]	0.0	0.0	0.3	0.0	0.0	8.4	7.1	8.2	12.3	9.3	2.7	1.9	2.3	7.9	2.7	20.5	6.7	9.4	7.5	11.0
BR (n = 25)																				
Average	1245.0	1338.8	1506.4	1593.0	1609.3	56.8	246.6	40.2	185.2	151.4	213.5	99.3	172.8	50.6	31.0	16105.5	33846.9	7677.5	14640.0	5005.8
Median	1245.0	1338.8	1506.3	1593.0	1609.1	57.4	245.5	40.4	190.5	148.4	213.7	99.7	173.3	50.0	31.1	16279.6	34466.1	7540.1	14995.5	4870.9
O.S.	0.0	0.6	1.8	0.0	0.5	6.3	25.9	5.3	28.1	18.8	1.7	1.9	1.9	1.6	1.1	1753.8	3543.6	993.0	1899.9	704.1
Co.V. [%]	0.0	0.0	0.1	0.0	0.0	11.0	10.5	13.3	15.2	12.4	0.8	1.9	1.1	3.1	3.6	10.9	10.5	12.9	13.0	14.1
CZ26 (n = 24)																				
Average	1245.0	1339.6	1501.7	1589.9	1604.0	84.0	419.3	62.6	167.9	331.6	202.8	96.2	148.0	77.5	37.2	20007.9	54774.9	11934.3	16158.0	13254.3
Median	1245.0	1339.4	1495.4	1588.4	1603.8	86.0	419.1	63.0	162.5	345.0	208.1	94.7	150.8	83.5	37.7	19710.2	55968.7	11924.5	16191.0	13886.1
SD	0.0	0.7	11.9	2.7	1.7	14.2	51.1	9.8	44.5	45.4	20.4	5.7	17.0	10.3	1.7	4371.4	6223.7	2458.2	3317.8	1993.6
Co.V. [%]	0.0	0.1	0.8	0.2	0.1	16.9	12.2	15.7	26.5	13.7	10.0	6.0	11.5	13.2	4.6	21.8	11.4	20.6	20.5	15.0
HOZ (n = 25)																				
Average	1245.0	1344.8	1537.0	1593.0	1612.7	48.4	579.3	47.3	299.7	170.2	229.7	70.6	137.2	41.4	32.8	11918.7	59632.9	7477.7	19373.1	6020.0
Median	1245.0	1344.9	1535.6	1592.8	1613.1	49.9	626.5	47.9	323.2	178.6	233.1	70.9	138.1	40.9	32.1	12527.9	63066.6	6923.0	20831.3	6070.1
SD	0.0	0.8	6.1	0.9	1.7	9.8	134.4	7.6	66.6	36.5	14.1	5.6	7.1	4.0	2.5	2672.5	10408.5	1606.8	3754.7	1323.9
Co.V. [%]	0.0	0.1	0.4	0.1	0.1	20.4	23.2	16.1	22.2	21.4	6.1	8.0	5.2	9.7	7.6	22.4	17.5	21.5	19.4	22.0
SOS																				
Average	1245.0	1340.1	1524.6	1593.0	1608.5	157.0	688.9	132.4	458.3	399.7	226.2	84.4	147.2	45.3	32.7	33204.8	76914.7	14105.4	28371.2	12184.8
Median	1245.0	1340.1	1526.7	1593.0	1608.7	114.4	679.1	75.9	423.0	352.2	227.2	84.2	150.4	43.8	32.6	33454.5	78333.5	14478.9	28965.2	12624.9
SD	0.0	0.6	6.3	0.0	1.4	226.9	142.7	286.3	247.3	255.5	3.4	1.7	7.3	6.0	1.3	3096.5	6051.2	1488.7	2619.1	2061.1
Co.V. [%]	0.0	0.0	0.4	0.0	0.1	144.5	20.7	216.2	54.0	63.9	1.5	2.0	5.0	13.3	3.9	9.3	7.9	10.6	9.2	16.9
TES (n = 27)																				
Average	1245.0	1346.3	1534.5	1593.9	1614.9	36.1	412.5	35.5	228.5	131.9	154.1	73.2	121.8	39.9	30.8	8173.1	44191.3	6049.0	14230.8	4703.3
Median	1245.0	1346.3	1534.5	1593.9	1615.1	36.1	416.2	34.3	231.5	133.5	154.3	72.3	123.9	39.4	31.4	8260.2	44467.9	6213.6	14308.0	4781.7
SD	0.0	0.5	4.2	1.4	1.5	4.5	61.8	7.5	37.9	15.6	1.1	5.7	7.6	1.8	3.4	1117.8	5132.3	1775.0	2083.6	574.8
Co.V. [%]	0.0	0.0	0.3	0.1	0.1	12.5	15.0	21.1	16.6	11.8	0.7	7.8	6.3	4.5	10.9	13.7	11.6	29.3	14.6	12.2
CZ51 (n = 25)																				
Average	1245.0	1344.3	1533.9	1592.9	1612.6	52.1	606.3	47.3	329.1	189.9	154.3	74.1	132.8	41.2	32.1	10621.1	65393.9	6880.0	21163.7	6789.5
Median	1245.0	1344.4	1535.1	1592.7	1612.8	52.4	609.1	47.1	331.3	194.9	154.3	73.3	133.1	40.7	32.6	10728.3	66800.9	6847.9	21162.9	6797.0
SD	0.0	0.8	3.4	1.0	1.3	5.2	93.5	5.2	40.2	17.3	0.0	5.9	1.8	2.0	2.8	1077.8	5977.3	819.8	1901.2	572.6
Co.V. [%]	0.0	0.1	0.2	0.1	0.1	9.9	15.4	11.0	12.2	9.1	0.0	7.9	1.3	4.8	8.7	10.1	9.1	11.9	9.0	8.4
CZ78 (n = 25)																				
Average	1245.0	1342.3	1526.6	1592.0	1610.8	62.2	556.5	54.4	336.5	217.3	227.3	80.7	142.1	43.0	32.3	15188.8	64889.8	8377.9	23117.9	7487.4
Median	1245.0	1342.4	1526.2	1591.9	1610.8	64.7	573.2	54.6	348.0	227.7	227.4	79.7	141.5	42.7	32.2	15876.9	66813.6	8214.0	23657.3	7676.8
SD	0.0	0.6	3.7	0.9	0.9	8.5	91.3	8.1	50.7	29.6	2.6	4.9	3.5	2.2	0.9	2073.2	8601.1	1264.7	3011.4	983.6
Co.V. [%]	0.0	0.0	0.2	0.1	0.1	13.6	16.4	14.8	15.1	13.6	1.2	6.0	2.4	5.2	2.8	13.6	13.3	15.1	13.0	13.1

SD – standard deviation; Co.V. – coefficient of variation = (SD/average) × 100; n.m. – not measured

Sample	Centre					Height					FWHH					Area				
	D4	D1	D3	G	D2	D4	D1	D3	G	D2	D4	D1	D3	G	D2	D4	D1	D3	G	D2
CZ66 (n = 25)																				
Average	1245.0	1345.3	1530.2	1593.5	1613.3	34.9	365.8	33.2	194.8	127.1	232.9	76.6	138.2	45.1	33.3	9264.8	40873.5	5295.6	13565.4	4557.1
Median	1245.0	1345.1	1530.3	1593.3	1613.0	37.1	365.6	37.0	203.0	129.5	230.1	77.8	139.3	45.0	33.3	9771.4	43520.8	5824.8	15152.0	4648.8
SD	0.0	0.8	4.2	1.2	1.5	11.4	147.0	10.1	71.5	41.1	8.9	6.7	7.4	3.0	1.8	3380.0	13533.8	1778.9	4375.5	1454.9
Co.V. [%]	0.0	0.1	0.3	0.1	0.1	32.7	40.2	30.6	36.7	32.4	3.8	8.7	5.3	6.8	5.5	36.5	33.1	33.6	32.3	31.9
CZ30 (n = 25)																				
Average	1245.0	1342.4	1517.2	1586.6	1608.0	56.4	403.0	45.9	195.0	239.5	213.1	86.0	142.0	54.2	36.1	14301.0	49376.8	9074.3	15223.3	9720.4
Median	1245.0	1342.1	1522.2	1592.0	1608.6	56.7	422.0	47.7	204.9	233.1	215.7	85.7	144.9	48.8	34.4	14499.4	51088.3	8508.0	16245.4	8556.7
SD	0.0	1.3	13.7	10.9	3.5	12.8	78.4	11.7	79.0	80.2	9.3	5.7	16.2	12.7	4.2	3573.2	9327.9	3447.4	4284.0	4608.9
Co.V. [%]	0.0	0.1	0.9	0.7	0.2	22.7	19.5	25.4	40.5	33.5	4.4	6.7	11.4	23.5	11.7	25.0	18.9	38.0	28.1	47.4
POK2 (n = 6)																				
Average	n.m.	1356.0	n.m.	1587.9	1623.7	n.m.	51.8	n.m.	54.7	9.0	n.m.	41.5	n.m.	32.2	21.3	n.m.	3424.2	n.m.	2901.2	228.6
Median	n.m.	1356.2	n.m.	1589.0	1625.6	n.m.	33.5	n.m.	42.5	5.7	n.m.	40.1	n.m.	32.5	18.7	n.m.	3049.9	n.m.	3197.1	214.4
SD	n.m.	2.4	n.m.	2.6	4.2	n.m.	32.6	n.m.	34.5	5.8	n.m.	4.5	n.m.	3.1	9.3	n.m.	1951.1	n.m.	1623.2	145.1
Co.V. [%]	n.m.	0.2	n.m.	0.2	0.3	n.m.	62.9	n.m.	63.2	64.5	n.m.	10.8	n.m.	9.6	43.5	n.m.	57.0	n.m.	55.9	63.5
ZLH (n = 20)																				
Average	n.m.	1351.2	n.m.	1583.7	1618.0	n.m.	67.6	n.m.	62.0	14.6	n.m.	41.1	n.m.	34.0	19.6	n.m.	4048.7	n.m.	3015.1	361.2
Median	n.m.	1351.2	n.m.	1583.9	1620.6	n.m.	43.9	n.m.	45.6	11.5	n.m.	39.9	n.m.	31.4	19.6	n.m.	2687.4	n.m.	2094.5	307.6
SD	n.m.	0.8	n.m.	1.2	6.6	n.m.	64.8	n.m.	44.8	11.7	n.m.	4.9	n.m.	8.8	7.5	n.m.	3634.8	n.m.	2031.4	254.8
Co.V. [%]	n.m.	0.1	n.m.	0.1	0.4	n.m.	95.8	n.m.	72.2	80.3	n.m.	12.0	n.m.	26.0	38.2	n.m.	89.8	n.m.	67.4	70.5

SD – standard deviation; Co.V. – coefficient of variation = (SD/average) × 100; n.m. – not measured

ples (Tab. 2; Fig. 5). FWHM-D1 in samples POK2 and ZLH is 39.1 cm^{-1} and 41.2 cm^{-1}, respectively, while other samples are in the range 70–123.8 cm^{-1}. FWHM-G in samples POK2 and ZLH is 27.4 and 30.0 cm^{-1}, respectively, while in other samples they are in the range 39.9–77.5 cm^{-1}. FWHM-D2 varies from 19.5–37.2 cm^{-1} and there is also no jump in values as in FWHM-D1. There is no distinguishable D4-band in samples POK2 and ZLH (Fig. 5).

The characteristics of Raman spectra (Tab. 2) imply that the temperature was below 330 °C (see Beyssac *et al.*, 2003a, b; Kouketsu *et al.*, 2014), except for ZLH and POK2 from the NW area of the Culm Basin (Andělská Hora Formation). The temperatures calculated from R2 ratios (Beyssac *et al.*, 2002a) are 324–420 °C. Very similar results are obtained using the Aoya *et al.* (2010) formula: 326–423 °C. However, both methods are not sensitive below 330 °C (Figs 6, 7); therefore, these estimates are not reliable (except for samples ZLH and POK2). Beyssac *et al.* (2002a) noted that for R2 values around 0.7 or higher it is only possible to state that the temperature was below 330 °C. Therefore, the Beyssac *et al.* (2002a) method only gives good results for temperature estimates in the range of ~300–650 °C for medium- or high-grade metamorphism (Beyssac *et al.*, 2002a, b; Aoya *et al.*, 2010; Kouketsu *et al.*, 2014). Above a temperature of 300 °C, both the Kouketsu *et al.* (2014) and Beyssac *et al.*, (2002a) methods produce similar results (Fig. 6). It is important to emphasise that the Raman spectra of very disordered OM are significantly different from and more complex than the spectra published in the systematic studies of OM structural evolution that are focused on higher-grade metamorphic rocks (i.e., typical greenschists and above; e.g., Wopenka and Pasteris, 1993; Beyssac *et al.*, 2002a, b). In such poorly crystallised OM, the use of R2 for characterisation is not appropriate, because the extension of coherent domains constituted by the aromatic rings is too small (Beyssac *et al.*, 2002a, b), while the application of the RA1 and RA2 ratios (Lahfid *et al.*, 2010) could cause overestimation of the temperature by 50–100 °C at temperatures outside a range of 200–300 °C (Kouketsu *et al.*, 2014: their fig. 7). The temperatures estimated using RA1 and RA2 differ by 50–200 °C from those of Kouketsu *et al.* (2014) for samples outside the interval of 240–340 °C (Tab. 3; Fig. 7C, D). Moreover, even the lithologies of samples CZ6, CZ39 and SV do not indicate medium- or high-grade metamorphism, as might be suggested by the Lahfid *et al.* (2010) method, but rather diagenesis to a very low metamorphic grade (Fig. 7C, D). Furthermore, above 340 °C the Lahfid *et al.* (2010) method indicates very low temperatures (~150 °C) for samples ZLH and POK2 from phyllites in the NW part of the study area, by comparison with ~390 °C derived from the formula of Kouketsu *et al.* (2014). For these two samples, the Beyssac *et al.* (2002a) formula gives temperature values similar to those from application of the Kouketsu *et al.* (2014) formula (Figs 6, 7). Therefore, the present authors did not use the Lahfid *et al.* (2010) approach for temperature estimation.

The Raman-derived maximum palaeotemperatures (T_{RSOM}), based on the Kouketsu *et al.* (2012) method, vary from 212 °C (sample Bu) up to 394 °C (ZLH sample) (Fig. 5). The maximum palaeotemperatures for rocks in the eastern region were ~210–240 °C (mainly in the Hradec-Kyjovice Formation), while the maximum palaeotemperatures in the central region were ~260–300 °C (in the Horní Benešov and Moravice formations). The highest palaeotemperatures affected the western areas (the Andělská Hora Formation and in part the Horní Benešov Formation), where

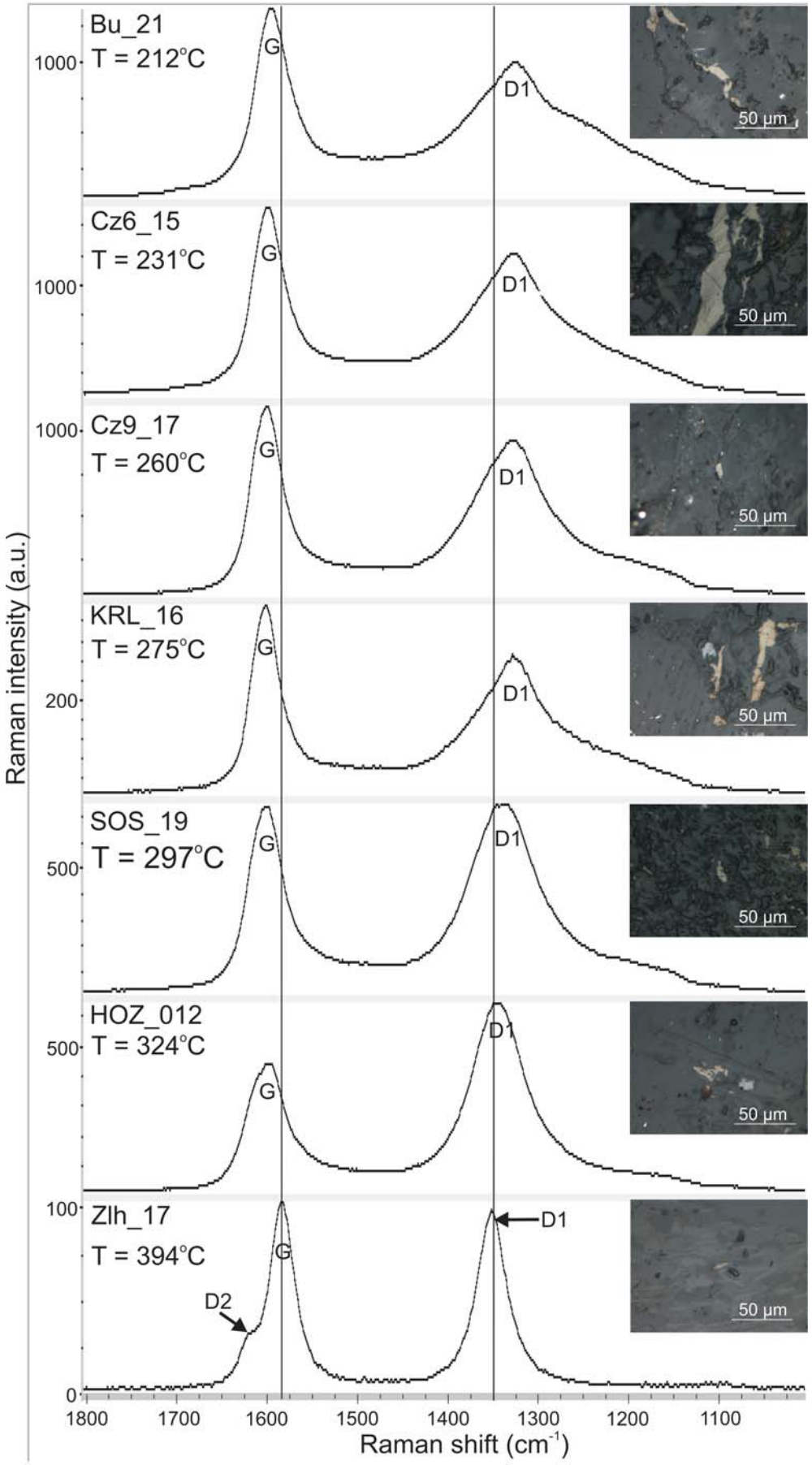

Fig. 5. Examples of measured Raman spectra of organic matter with photographs.

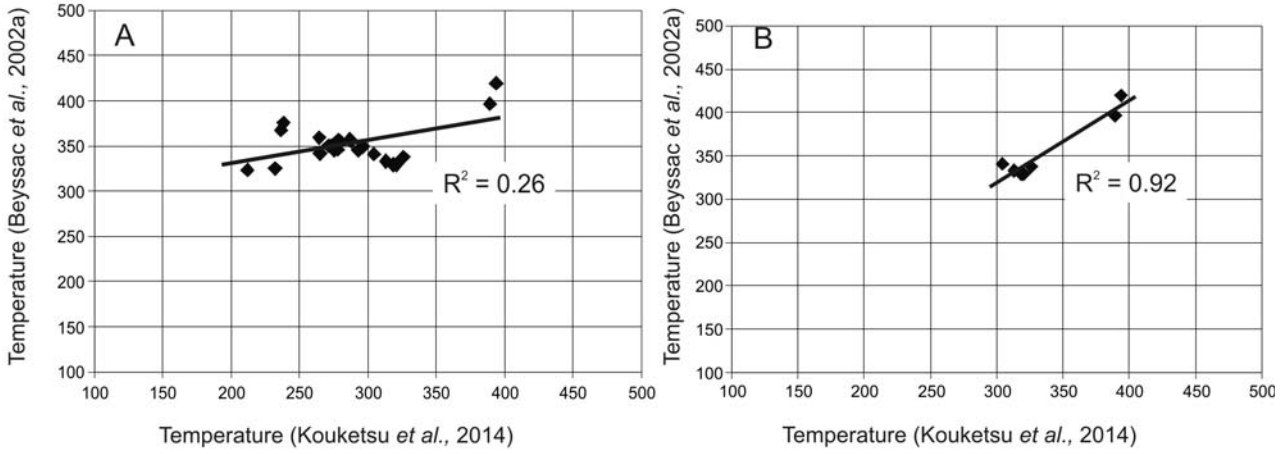

Fig. 6. Comparison of maximum palaeotemperatures calculated from the Raman spectra using the Beyssac *et al.* (2002a) and Kouketsu *et al.* (2014) approaches. **A.** All samples. **B.** Samples having temperature higher than 310 °C. See further explanation in the text.

they reached ~280–330 °C and even up to almost 390 °C in the most NW corner of the Culm Basin. The Raman-derived maximum palaeotemperatures agree relatively well with the burial-related temperatures in the E of the Culm Basin, while in the W of Culm Basin T_{RSOM} corresponds to the hydrothermal-related temperature (Fig. 4).

Fluid inclusions in the veins

Greywackes and shales contain steeply dipping (60–80°) joints, filled with quartz and/or calcite, the thickness of which does not exceed 5 cm. Microthermometric measurements were performed on primary fluid inclusion assemblages (FIA). They form densely packed areas or belts, arranged along the host-crystal growth zones (Fig. 9A). The size of the inclusions varies from a few to about 10 μm. Small inclusions have rounded contours, whereas the large ones are more irregular, sometimes elongated or C-shaped. Some of the inclusions contain small channels, which indicate the unsealing of inclusions. Such inclusions have different liquid-to-gas (L-to-G) ratios than other inclusions and are mostly gaseous or predominantly gaseous. In samples Cz74 and SV, the primary FIAs are sparse and occupy small, irregular areas. In both samples, secondary FIAs predominate with a variable phase ratio and form linear assemblages of very small sizes (Fig. 9B).

The pressure-temperature-molar-volume-composition (P-T-V-X) properties of the fluid inclusions differ in various parts of the Culm Basin. In its NW part (sample Cz54, located very close to sample POK2), the primary FIAs in quartz veins are in the liquid-gas (LG) phase with a constant G/L ratio of ~30 vol.%. Raman microspectrometry revealed that such inclusions are filled with CO_2 in both the liquid and gas phases (Fig. 9C, D). In all the inclusions, these peaks show a down-shift of ~3 cm^{-1}, which indicates a high density (low molar volume) of CO_2 (Burke, 2001). The microthermometric measurements support this conclusion. The homogenisation temperature (Th) is mainly in the range of 26.2–28.3 °C (Fig. 9E). In two inclusions, the Th is 20.7 and 30.0 °C. The calculations of the homogenisation pressures and molar volumes of CO_2 according to Bakker (2009, 2012) give values in the ranges of 5.8–7.2 MPa and 57.47–74.18 cm^3/mol, respectively.

The secondary FIAs are also two-phase, but with a highly variable G/L ratio. The Raman analyses indicate the aqueous character of these inclusions. Only in a few cases does the vapour phase contain a small amount of CO_2 (weak intensity of peaks at 1285 and 1388 cm^{-1}).

In the central part of the basin (sample Cz9; calcite), the primary FIAs are the liquid-gas (LG) phase with a constant G/L ratio of 20–30 vol.%. In Raman microspectrometry, they show an aqueous character mostly without any visible dissolved gases. Only in a few cases was methane found in gas bubbles (peak at 1712 cm^{-1}, Fig. 9F). The down-shift of this peak indicates a high density of CH_4 (Burke, 2001). The homogenisation temperature for the inclusions without CH_4 is in the range 305.7–367.3 °C, which indicates that the molar volumes vary from 26.1 to 32.1 cm^3/mol. The distribution of Th approximates the normal one (Fig. 10A).

Towards the E (sample Cz74; quartz), the range of Th in primary FIAs is considerably wider (173.6–404.1 °C) and the distribution of Th is not normal (Fig. 10B). In the eastern part of the basin (sample SV; quartz), Th is in the range of 207.9–315.4 °C and the data distribution evidently is not normal (Fig. 10C). In both samples, CH_4 frequently occurs in the gas phase of the inclusions, as confirmed by Raman microspectrometry. The amount of CH_4 is variable, according to various heights of the peak at ~2917 cm^{-1} (Fig. 10D). The inclusions with high amounts of CH_4 also contain a small amount of CO_2 (Fig. 10D, upper spectrum). The Raman down-shift of the CH_4 and CO_2 peaks is significant (Tab. 4). In sample Cz74, the methane band position is down-shifted up to 6.1 cm^{-1} and in sample SV up to 8.1 cm^{-1}. Applying the Burke (2001) data, the fluid pressure in measured inclusions is estimated to be between 7 and 300 MPa.

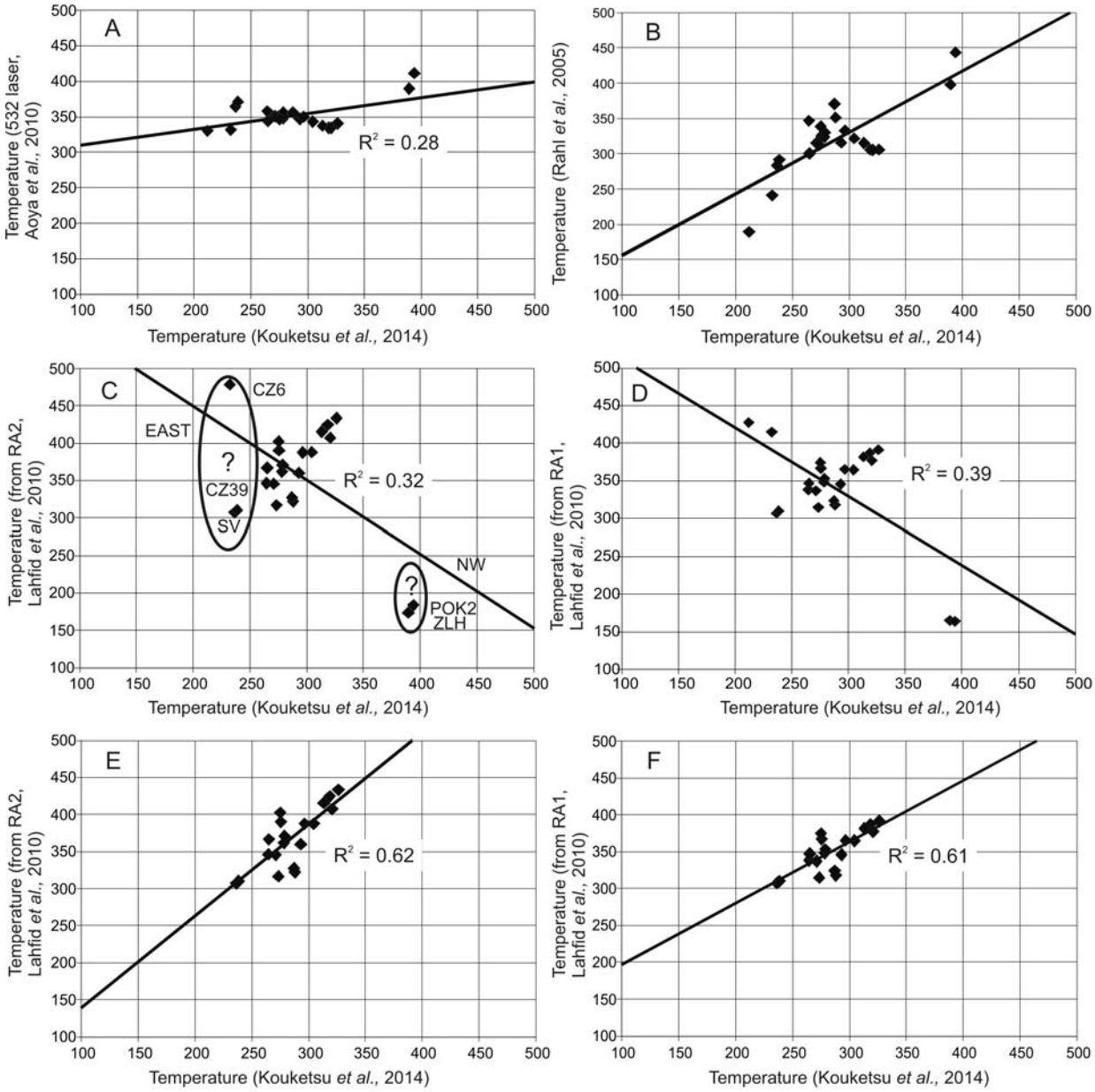

Fig. 7. Comparison of maximum palaeotemperatures calculated from the Raman spectra using formulae of Rahl *et al.* (2005), Aoya *et al.* (2010), Lahfid *et al.* (2010) and Kouketsu *et al.* (2014). **A–D.** All samples. **E.** Samples in range 240–340 °C using RA2. **F.** Samples in range 240-340 °C using RA1. See further explanation in the text.

DISCUSSION

Thermal maturity of organic matter

In the lower maturity range (approximate diagenesis zone), where the various macerals could be readily identified, the measurements are restricted to vitrinite fragments (i.e., vitrodetrinite), but in high-rank material (e.g., in anchizone and epizone) such a restriction is not always possible (Diesel and Offler, 1975; Diesel *et al.*, 1978). This might be the reason for the wider range of vitrinite reflectance values (Diesel and Offler, 1975; Diesel *et al.*, 1978; Dvořák and Wolf, 1979; Dvořák, 1989). Occasionally, in some samples with lower-rank organic particles, a transitional material ("graphite-like", according to Diesel and Offler, 1975; Diesel *et al.*, 1978; Suchý *et al.*, 1997, 2015) is present, particularly in the western part of the study area (Fig. 3E, F). It is probably of detrital origin. Rare coke-like structures are also in some phytoclasts, similar to those reported by Diessel and Offler (1975) and Diesel *et al.* (1978). Suchý *et al.* (1997, 2015) suggest that the origin of such high-reflecting organic particles is ambiguous and both the detrital contribution of recycled material and an authigenic phase are possible. However, the relationships between its occurrence and tectonic deformation of the enclosing sediments indicate that localised tectonic pressures might have been involved (e.g., Bustin *et al.*, 1986; Suchý *et al.*, 1997, 2015; Littke *et al.*, 2012).

At high levels of coalification and graphitisation, the lithology of the surrounding rocks, heating rate, tectonic stress (pressure) and possible changes of thermal conductiv-

Table 3

Maximum palaeotemperature estimations, based on the Raman data

Sample	Kouketsu *et al.* (2014)	Beyssac *et al.* (2002a)			Aoya *et al.* (2010)		Rahl *et al.* (2005)	Lahfid *et al.* (2010)			
	Temp.1	R1	R2	Temp. from R2	532 mm Temp.1	514 mm Temp.2	Temp. from R1 & R2	RA1	RA2	Temp. from RA1	Temp. from RA2
Bu											
Average	211.9	0.8	0.7	323.7	330.4	326.1	189.6	0.7	2.5	427.6	506.2
Median	211.2	0.8	0.7	324.5	331.0	326.9	184.2	0.7	2.6	429.1	508.9
SD	20.4	0.1	0.0	6.6	4.8	6.4	29.3	0.0	0.1	11.5	25.2
Co.V. [%]	9.6	11.9	2.1	2.1	1.5	1.9	15.4	1.3	4.5	2.7	5.0
SV											
Average	238.5	0.8	0.6	375.8	371.2	377.3	291.5	0.6	1.7	310.3	310.4
Median	239.9	0.7	0.6	377.9	372.8	379.3	277.7	0.6	1.6	302.5	299.2
SD	10.5	0.4	0.0	9.0	7.6	9.1	43.6	0.0	0.1	24.0	30.5
Co.V. [%]	4.4	48.1	3.4	2.4	2.0	2.4	15.0	3.1	8.2	7.7	9.8
CZ39											
Average	236.4	0.8	0.6	367.8	364.6	369.3	283.9	0.6	1.7	307.0	307.1
Median	234.5	0.8	0.6	370.3	366.6	371.8	286.6	0.6	1.7	310.6	309.3
SD	12.7	0.1	0.0	10.3	8.3	10.3	28.0	0.0	0.2	29.4	38.7
Co.V. [%]	5.4	8.5	3.8	2.8	2.3	2.8	9.9	3.8	10.5	9.6	12.6
CZ74											
Average	265.1	1.3	0.7	342.1	344.1	343.9	300.5	0.7	1.9	347.1	366.8
Median	264.2	1.3	0.7	341.8	343.8	343.5	298.2	0.7	2.0	361.4	381.0
SD	9.2	0.3	0.0	4.7	3.6	4.6	17.7	0.0	0.3	48.9	71.1
Co.V. [%]	3.5	20.8	1.6	1.4	1.0	1.3	5.9	6.0	16.7	14.1	19.4
CZ74_thin-sec.											
Average	273.4	1.3	0.7	350.1	350.3	351.7	312.7	0.6	1.7	314.8	316.8
Median	272.3	1.2	0.7	348.2	348.8	349.8	304.7	0.6	1.6	305.1	302.4
SD	3.9	0.2	0.0	6.5	5.2	6.4	27.7	0.0	0.2	27.8	39.2
Co.V. [%]	1.4	14.0	2.2	1.9	1.5	1.8	8.9	3.5	10.4	8.8	12.4
CZ6											
Average	232.3	1.1	0.7	325.4	331.6	327.7	241.3	0.7	2.4	414.9	478.7
Median	234.9	1.1	0.7	325.6	331.8	328.0	243.3	0.7	2.4	412.9	474.0
SD	12.1	0.1	0.0	5.8	4.2	5.5	21.5	0.0	0.1	9.4	20.1
Co.V. [%]	5.2	10.9	1.8	1.8	1.3	1.7	8.9	1.1	3.7	2.3	4.2
CZ9											
Average	278.7	1.3	0.6	356.9	355.6	358.4	330.6	0.7	1.9	353.0	371.1
Median	280.0	1.2	0.6	357.9	356.4	359.4	332.4	0.6	1.8	334.3	340.7
SD	4.5	0.1	0.0	5.0	4.0	5.0	17.4	0.0	0.2	29.8	47.0
Co.V. [%]	1.6	8.5	1.8	1.4	1.1	1.4	5.3	3.6	10.9	8.4	12.7
CZ4											
Average	278.2	1.6	0.7	346.2	347.3	347.9	323.6	0.7	1.9	348.1	361.7
Median	278.8	1.5	0.7	349.0	349.4	350.6	322.9	0.7	1.9	353.0	368.0
SD	4.7	0.4	0.0	6.1	4.7	6.0	19.4	0.0	0.1	18.5	27.9
Co.V. [%]	1.7	24.6	2.1	1.8	1.4	1.7	6.0	2.3	6.6	5.3	7.7
CZ19											
Average	275.6	1.3	0.7	350.6	350.6	352.2	325.0	0.7	2.0	366.9	390.1
Median	276.2	1.3	0.7	351.1	351.0	352.6	325.0	0.7	2.0	363.3	384.1
SD	3.4	0.1	0.0	3.1	2.4	3.0	10.0	0.0	0.1	10.1	16.7
Co.V. [%]	1.3	6.4	1.1	0.9	0.7	0.9	3.1	1.2	3.7	2.7	4.3
DVO											
Average	288.0	1.7	0.6	355.7	354.8	357.2	351.2	0.6	1.7	317.9	322.3
Median	281.0	1.6	0.6	355.3	354.3	356.8	357.8	0.6	1.7	318.1	318.8
SD	27.2	0.4	0.0	13.0	10.7	13.0	25.8	0.0	0.2	37.9	48.4
Co.V. [%]	9.5	24.5	4.5	3.6	3.0	3.6	7.4	4.8	12.7	11.9	15.0

Sample	Kouketsu *et al.* (2014)	Beyssac *et al.* (2002a)			Aoya *et al.* (2010)		Rahl *et al.* (2005)	Lahfid *et al.* (2010)			
	Temp.1	R1	R2	Temp.	532 mm	514 mm	Temp.	RA1	RA2	Temp.	Temp.
				from R2	Temp.1	Temp.2	from R1 & R2			from RA1	from RA2
KRL											
Average	275.2	1.6	0.7	345.8	347.0	347.5	338.7	0.7	2.1	374.5	402.5
Median	275.1	1.6	0.7	346.1	347.1	347.8	340.2	0.7	2.1	373.9	401.4
SD	9.9	0.1	0.0	5.1	3.9	4.9	14.4	0.0	0.1	6.9	11.9
Co.V. [%]	3.6	4.6	1.7	1.5	1.1	1.4	4.2	0.8	2.6	1.8	3.0
KUN											
Average	287.1	1.8	0.6	357.3	356.0	358.8	370.7	0.6	1.7	323.9	327.2
Median	286.9	1.8	0.6	356.3	355.2	357.8	370.7	0.6	1.7	321.0	322.7
SD	3.6	0.2	0.0	4.1	3.2	4.0	13.1	0.0	0.1	15.9	22.1
Co.V. [%]	1.2	10.0	1.4	1.1	0.9	1.1	3.5	2.0	5.7	4.9	6.7
BR											
Average	264.5	1.3	0.6	359.5	357.7	360.9	346.9	0.6	1.8	338.4	346.5
Median	263.7	1.3	0.6	359.1	357.4	360.6	347.2	0.6	1.8	338.8	347.1
SD	4.1	0.1	0.0	2.7	2.2	2.7	11.9	0.0	0.0	6.4	9.0
Co.V. [%]	1.6	8.4	1.0	0.8	0.6	0.7	3.4	0.8	2.2	1.9	2.6
CZ26											
Average	271.1	2.6	0.7	351.4	351.4	353.0	315.4	0.6	1.8	335.0	342.1
Median	274.5	2.7	0.6	354.7	353.9	356.3	326.6	0.6	1.8	334.7	341.2
SD	12.3	0.5	0.0	9.4	7.2	9.1	62.4	0.0	0.1	13.1	19.0
Co.V. [%]	4.6	17.6	3.2	2.7	2.0	2.6	19.8	1.6	4.7	3.9	5.5
HOZ											
Average	326.2	1.9	0.7	328.8	334.1	331.0	305.8	0.7	2.2	385.4	422.1
Median	325.5	1.9	0.7	329.5	334.6	331.7	309.3	0.7	2.2	390.6	430.6
SD	12.1	0.2	0.0	5.9	4.3	5.6	13.8	0.0	0.1	13.6	23.6
Co.V. [%]	3.7	8.0	1.9	1.8	1.3	1.7	4.5	1.6	4.9	3.5	5.6
SOS											
Average	296.6	1.6	0.7	349.8	350.1	351.4	332.7	0.7	2.0	365.3	387.7
Median	297.0	1.6	0.7	348.5	349.0	350.1	339.4	0.7	2.0	367.9	391.4
SD	3.7	0.5	0.0	5.9	4.7	5.8	32.5	0.0	0.1	11.1	16.3
Co.V. [%]	1.2	27.5	2.0	1.7	1.3	1.6	9.8	1.3	3.6	3.0	4.2
TES											
Average	320.7	1.8	0.7	329.4	334.6	331.6	305.6	0.7	2.1	377.0	407.4
Median	322.5	1.8	0.7	329.1	334.3	331.3	304.9	0.7	2.1	377.4	407.4
SD	12.3	0.1	0.0	2.9	2.2	2.8	5.5	0.0	0.1	14.2	23.7
Co.V. [%]	3.8	7.8	0.9	0.9	0.6	0.9	1.8	1.7	5.1	3.8	5.8
CZ51											
Average	318.7	1.8	0.7	329.4	334.5	331.6	305.9	0.7	2.2	387.1	424.8
Median	320.3	1.9	0.7	328.9	334.2	331.1	305.7	0.7	2.2	388.8	427.3
SD	12.6	0.1	0.0	3.0	2.2	2.9	5.0	0.0	0.1	10.4	18.5
Co.V. [%]	4.0	7.8	1.0	0.9	0.7	0.9	1.6	1.2	3.8	2.7	4.4
CZ78											
Average	304.5	1.7	0.7	338.7	341.5	340.6	321.9	0.7	2.1	370.7	396.4
Median	306.6	1.6	0.7	338.6	341.4	340.5	320.8	0.7	2.1	372.0	398.2
SD	10.4	0.1	0.0	3.4	2.6	3.3	7.5	0.0	0.1	8.7	14.3
Co.V. [%]	3.4	6.4	1.1	1.0	0.8	1.0	2.3	1.0	3.1	2.3	3.6
CZ66											
Average	313.2	1.9	0.7	333.2	337.4	335.2	315.3	0.7	2.1	381.8	415.5
Median	310.8	1.9	0.7	333.0	337.2	335.0	315.0	0.7	2.2	385.2	420.8
SD	14.4	0.1	0.0	3.4	2.5	3.3	7.1	0.0	0.1	13.7	23.3
Co.V. [%]	4.6	7.8	1.1	1.0	0.7	1.0	2.3	1.6	4.9	3.6	5.6
CZ30											
Average	293.0	2.5	0.7	345.7	346.9	347.4	315.5	0.7	1.9	344.6	357.9
Median	293.7	1.7	0.7	343.1	344.8	344.8	327.2	0.7	1.9	343.2	353.3
SD	12.3	1.4	0.0	8.2	6.4	8.0	36.9	0.0	0.2	27.9	41.0
Co.V. [%]	4.2	54.7	2.8	2.4	1.8	2.3	11.7	3.4	9.8	8.1	11.4
POK2											
Average	388.8	1.0	0.5	408.5	399.9	410.6	413.6	0.5	1.1	183.4	184.5

Sample	Kouketsu *et al.* (2014)	Beyssac *et al.* (2002a)			Aoya *et al.* (2010)		Rahl *et al.* (2005)	Lahfid *et al.* (2010)			
	Temp.1	R1	R2	Temp.	532 mm	514 mm	Temp.	RA1	RA2	Temp.	Temp.
				from R2	Temp.1	Temp.2	from R1 & R2			from RA1	from RA2
POK2											
Average	388.8	1.0	0.5	408.5	399.9	410.6	413.6	0.5	1.1	183.4	184.5
Median	391.9	1.0	0.5	408.4	399.7	410.5	412.9	0.5	1.1	183.6	183.3
SD	9.6	0.1	0.0	12.7	11.6	13.1	13.0	0.0	0.1	35.6	27.4
Co.V. [%]	2.5	14.3	5.4	3.1	2.9	3.2	3.1	5.4	11.2	19.4	14.8
ZLH											
Average	389.6	1.1	0.5	410.9	403.4	413.7	418.7	0.5	1.1	176.6	191.0
Median	392.3	0.9	0.5	412.5	403.4	414.7	418.9	0.5	1.1	172.2	174.6
SD	10.6	0.4	0.1	37.2	35.5	39.2	60.7	0.1	0.4	104.6	84.5
Co.V. [%]	2.7	42.4	16.2	9.1	8.8	9.5	14.5	16.2	33.7	59.2	44.2

SD – standard deviation; Co.V. – coefficient of variation = (SD/average) × 100 [%]

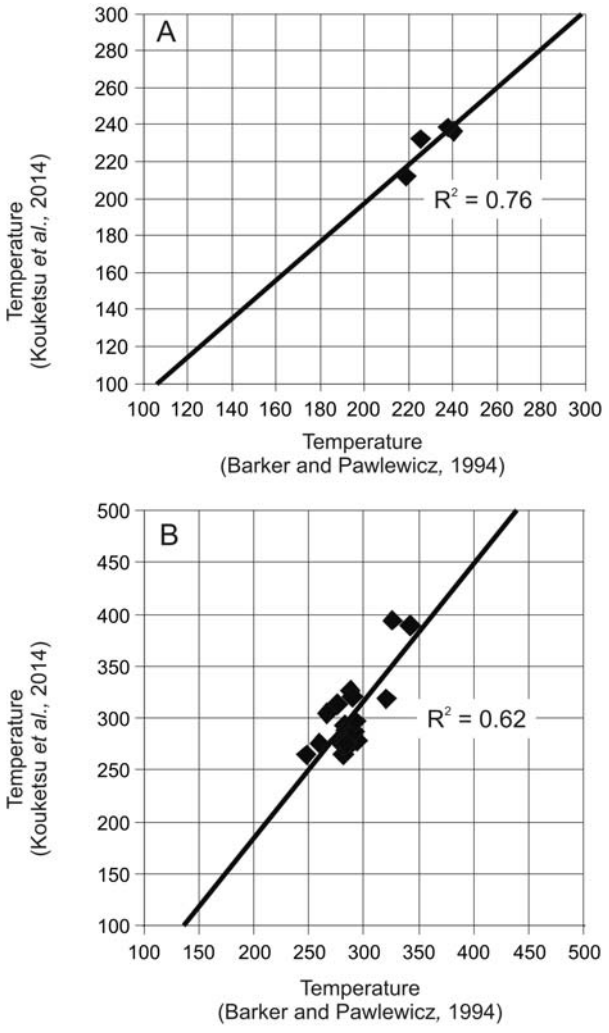

Fig. 8. Comparison of temperatures from Barker and Pawlewicz (1994) with the temperatures derived from the Raman spectra of organic matter (Kouketsu *et al.*, 2014). **A.** Temperatures in the eastern part of the basin (burial model of maturity). **B.** Temperatures in the central and western parts of the basin (hydrothermal model of maturity). See further explanation in the text.

Table 4

Band positions of CH_4 and CO_2 in samples Cz74 and SV

Sample Cz74		Sample SV			
No inclusion	Position CH_4 band	No inclusion	Position CH_4 band	v_1CO_2	$2v_2CO_2$
2	2915.1	2	2911.9		
3	2914.4	4	2913.5		
4	2912.8	7	2909.3		
5	2913.4	8	2909.4	1280.2	1383.1
6	2914.1	9	2909.2	1279.7	1383.4
8	2914.9	11	2908.9		
11	2915.4	12	2912.2		
12	2910.9	16	2909.3		
15	2913.4	17	2909.2		
18	2913.4	18	2909.5	1281.5	1383.3
Mean	2913.8		2910.2		
Median	2913.8		2909.4		
S.D.	1.318		1.637		
Co.V.	0.05		0.06		
Min	2910.9		2908.9		
Max	2915.4		2913.5		

S.D. – standard deviation; Co.V. – coefficient of variation = (S.D./average) × 100 [%]

ity during diagenesis should be considered (Suchý *et al.*, 1997, 2015; Barzoi, 2015; Bruns and Littke, 2015; Hartkopf-Fröder *et al.*, 2015), in addition to the major factors of temperature and time. Samples from the Culm Basin are characterised by high thermal maturation of OM (Dvořák and Wolf, 1979; Dvořák, 1989; Nowak, 2003; Bábek *et al.*, 2005, 2008; and this work). Vitrinite reflectance data also corroborate the observation that according to clay mineral diagenesis (Dvořák, 1989), the lower Carboniferous Culm samples are in the late diagenetic to anchimetamorphic range. Organic maturity and illite crystallinity data indicate maximum palaeotemperatures of ~200–350 °C for the Nízký Jeseník Culm Sub-basin (Dvořák, 1989). However, particularly in the western parts of the study area, vitrinite reflectance varies considerably, which is not yet fully understood. Bruns and Littke (2015) showed that a partially sig-

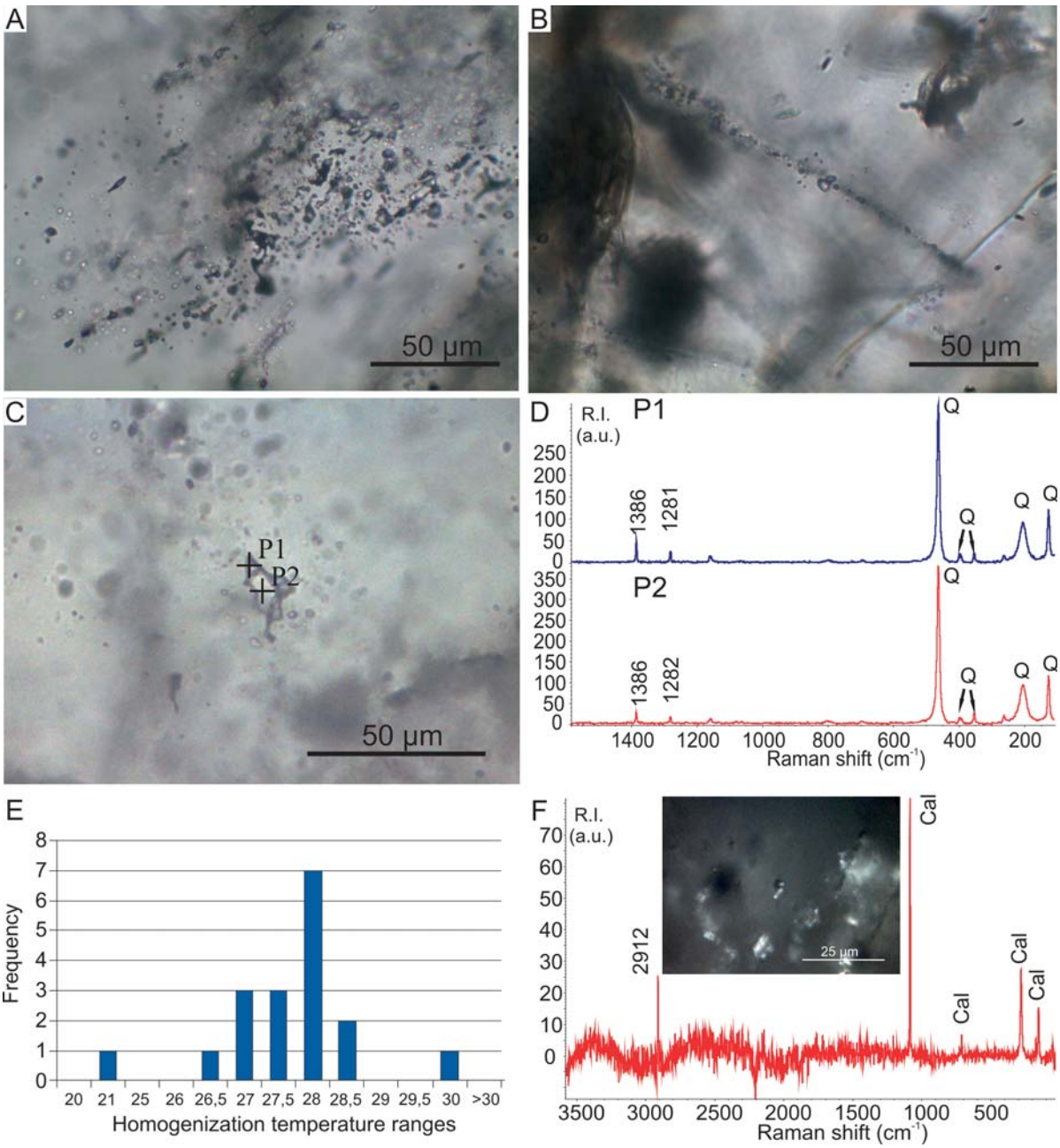

Fig. 9. Measurements of fluid inclusions. **A.** The areas of primary FIAs in calcite (sample Cz9). **B.** Secondary FIA in sample SV. **C.** A primary inclusion filled with liquid-gas CO_2: P1, P2 – measurement points. **D.** Raman spectra for the points P1 and P2. Raman intensities (RI) in arbitrary units. **E.** The homogenisation temperature histogram of sample Cz54. **F.** Raman spectrum of an inclusion with CH_4 (sample Cz9).

nificant scatter of vitrinite reflectance might arise in fine-grained rocks, not only owing to the high rank and associated anisotropic character, but also because of lithological variation (Tab. 1). VR_{max} is both pressure and temperature sensitive at this maturity stage (e.g., Suchý *et al.*, 1997). Thus, it cannot be easily converted to determine the maximum temperature that the OM experienced (Le Bayon, 2012; Le Bayon *et al.*, 2012), but instead it can be better used as a stress indicator (Bruns and Littke, 2015). Increasing temperature accelerates chemical reactions during maturation and thus controls the degree of aromatisation. This aromatisation in turn controls the refractive and adsorptive indices, upon which the reflectance depends. Pressure tends to promote physical-structural coalification, which affects the optical properties of vitrinite by enforcing the alignment of the sheet-like aromatic lamellae perpendicular to the principal maximum stress direction (Taylor *et al.*, 1998; Barzoi, 2015; Bruns and Littke, 2015). Therefore, taking into account the above consideration, the present authors applied only mean VR_r data for conversion into maximum palaeotemperature, using the Barker and Pawlewicz (1994) formulas. Generally, on a regional scale the temperature values calculated from VR_r values (Tab. 1; Fig. 4) agree with the previous estimations given by Dvořák (1989).

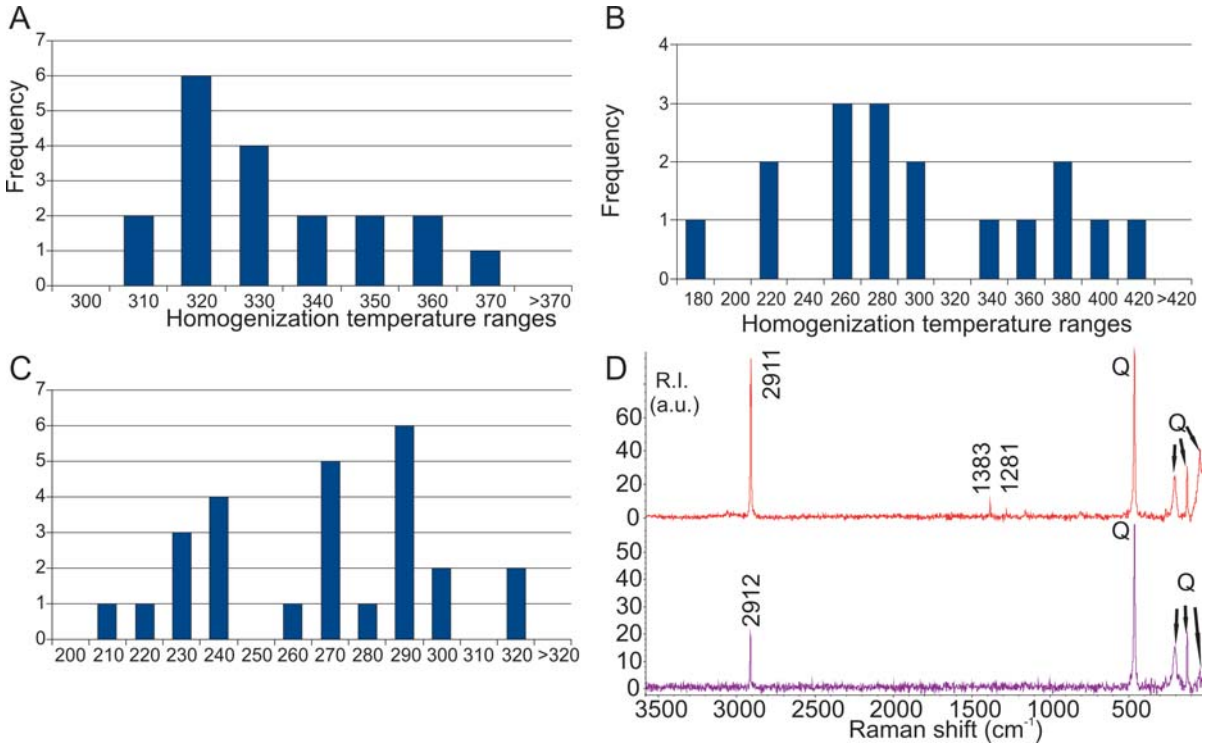

Fig. 10. Measurements of homogenisation temperatures. **A.** Histogram of sample Cz9. **B.** Histogram of sample Cz74. **C.** Histogram of sample SV. **D.** Raman spectra of inclusions in sample SV: upper – with a high amount of CH_4 and a minor amount of CO_2; lower – with a low amount of CH_4.

The Raman-derived maximum palaeotemperature (T_{RSOM}) shows increasing thermal maturity of OM from E to W and N-W in a considerably more systematic way than the VR_r data (Fig. 4). The T_{RSOM} is compatible with the VR_r-derived palaeotemperature, based on the burial model in the eastern area (samples CZ6, Bu, SV and CZ39), and with the VR_r-derived palaeotemperature, based on the hydrothermal model in the central and western areas (all other samples, Figs 4, 8). Such a distribution seems to be related to Variscan burial heating (e.g., sedimentary and/or tectonic; see Franců *et al.*, 2002, as in the Drahany Upland), overprinted later by a thermal event recorded mainly in the western and central parts of the Nízký Jeseník Culm Sub-basin (Fig. 4). It is also worth noticing that the study area is intersected by several major faults (Fig. 1) and some samples (e.g., HOZ, TES) are located close to them. These faults could act as active heat conduits in the tensional regime of the late to post-Variscan period (e.g., Kříbek *et al.*, 2009; Špacek *et al.*, 2015). Generally, in the MSFTB (Fig. 1; Rajlich, 1990; Hladil, 1994; Kalvoda, 1998; Hladil *et al.*, 1999; Kalvoda and Melichar, 1999; Schulmann and Gayer, 2000), which formed during the late phases of the Variscan collision (330–310 Ma), a significant fluid flow system was developed. It produced veins of mainly quartz and calcite that are partially ore-bearing (Kučera and Slobodnik, 2002; Zimák *et al.*, 2002; Dolníček *et al.*, 2014), as well as several important ore deposits (Kříbek *et al.*, 2009; Pohl, 2011). The MSFTB was reactivated in the Permian and Triassic owing to transtensional movements (Kříbek *et al.*, 2009). Kříbek *et al.* (2009) established the following stages of the post-contractional evolution of the MSFTB: (i) Variscan post-orogenic extension (~307–300 Ma, late Carboniferous), (ii) late Variscan transcurrent tectonics and Boskovice graben formation (~300–260 Ma, Permian) and (iii) final reactivation during early rifting in the Tethys-Central Atlantic region (~240–220 Ma, Triassic).

Zircon (U-Th/He) dating also supports the interpretation by the present authors (D. Botor, *unpub. data*). The zircon helium (ZHe) ages form a distinct spatial pattern and increase towards the E of the study area. The ZHe ages in the E range from 303.1 to 232.6 Ma (late Carboniferous to Early Triassic), but they are significantly younger in the W, ranging from 194.1 to 162.9 Ma (Early–Middle Jurassic). The ZHe ages are cooling ages, showing that the rocks traversed the 170–190 °C isotherm zone in the Early–Middle Jurassic in the western part of the study area. The radiometric data show that the western part of the Culm Basin probably was reheated in the post-Variscan period. However, the ZHe ages in the E of the Culm Basin, which range from 303.1 to 232.6 Ma (late Carboniferous to Early Triassic) show that maximum heating was reached in the Carboniferous Period. This is similar to the western part of the Upper Silesia Coal Basin (E of the Culm Basin), where apatite fission track and U-Th/He datings were used to exclude post-Variscan heating (Botor, 2014). Vamvaka *et al.* (2014), on the basis of an apatite fission track study in the southern part of the Bohemian Massif, concluded that a full explanation of the apatite fission track age record must consider higher crustal heat flow in the Mesozoic (Middle to Late Jurassic). This increase in heat could be caused by intense fault activity, either during crustal extension and lithospheric thinning, resulting in steeper geotherms, or by

flexural subsidence due to the overloaded crust (Vamvaka *et al.*, 2014); however, the latter hypothesis (subsidence) is unlikely considering the thin overburden in the study area (<200 m, Malkovský, 1987; McCann *et al.*, 2006). However, towards the NW of the study area (the Rychlebské Hory Mts. and the Rudawy Janowickie Mts.), Danišík *et al.* (2012) and Sobczyk *et al.* (2015) postulated a significant (>5–6 km) Cretaceous burial, based on ZHe dating.

Fluid inclusions

Fluid inclusions in the samples of calcite and quartz veins show two compositional types. In the NW part of the study area (sample CZ54), the inclusions are mostly filled with CO_2, probably accompanied by a very small amount of water, not visible under the microscope. Such inclusions represent a very low XH_2O (very high XCO_2) compositional type (Diamond, 2001), typical of high-grade metamorphic rocks. Within the Culm sediments, the mineral association and the thermal maturity of OM do not show such high-grade metamorphic alteration. Without doubt, the calcite veins were formed under hydrothermal conditions at high temperatures from migrating fluids from deeper parts of the crust that contained a low amount of molar volume (high density) of CO_2 (Mullis *et al.*, 1994). The present authors suppose that these fluids may have been partially enriched in CO_2 from OM decomposition (Mullis *et al.*, 1994) or of magmatic origin. This process led to a significant CO_2 concentration, similar to that of the high-grade metamorphic environment. The temperature estimated from Raman spectra is almost 400 °C. Taking into account isochores for the molar volumes 57.47–74.18 cm^3/mol and a temperature of 400 °C, the pressure of the fluid entrapment in inclusions is in the range 103.24–173.53 MPa (Fig. 11). Such pressures, assuming a confined pressure gradient equal to 0.023 MPa/m (e.g., Magara, 1978), correspond to a burial of about 4500–7500 m. Therefore, the calculated geothermal palaeogradients vary from 53 °C/km (for the 7500 m burial) to 88 °C/km (for 4500 m burial). Taking into account the palaeotectonic setting, a value of 53 °C/km seems to be most probable. Nevertheless, it is a high value, which seems to be a result of the influence of hydrothermal activity, which caused a second stage of coalification in the western part of the study area.

Within the central and eastern parts of the Culm Basin the FIAs are different. They are filled with aqueous solutions. In the central part (sample Cz9, Fig. 10A) the range of Th is lower than in the eastern part (samples CZ74 and SV; Fig. 10B, C). The composition of inclusions and Th indicate entrapment from homogeneous solutions and molar volumes suggest entrapment in high temperature and relatively low pressure conditions (see Roedder, 1984; Mullis *et al.*, 1994; Goldstein, 2001). In the higher temperature ranges (Fig. 11A), the distribution of Th is uniform, which may indicate that the inclusions are partly unsealed. Assuming geothermal gradients of 35, 50 and 65 °C/km (Fig. 12) and a burial temperature of 260 °C, as estimated from the Raman data, the burial depth was about 7.2, 5.0 and 3.8 km, respectively, and the confined pressure about 169.5, 116 and 89 MPa, respectively. Considering the pressure and Th in the

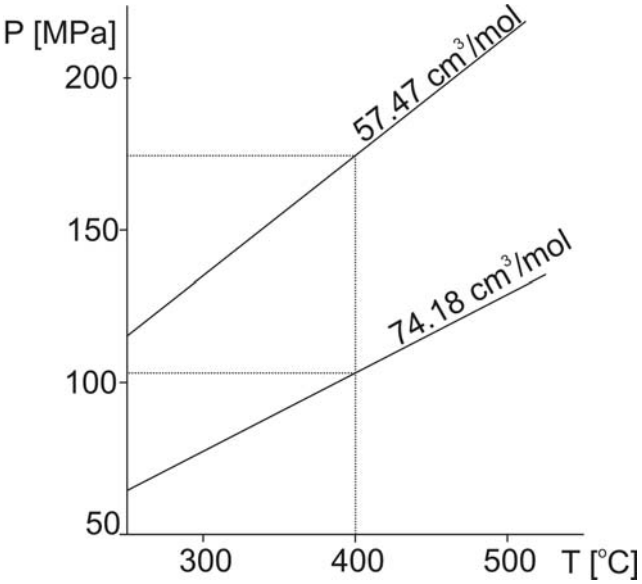

Fig. 11. P-T diagram with marginal isochores of pure CO_2 from an inclusion in sample Cz54 (calculation after Bakker, 2009, 2012).

range 306–340 °C, the temperatures of hydrothermal solutions should have been about 455–535 °C, 408–470 °C and 383–437 °C, respectively (Fig. 12; calculation based on Diamond, 2003; Bakker, 2009, 2012). For an estimate of geothermal gradients there is a discrepancy between the temperatures deduced from the OM estimations and from the hydrothermal solutions; however, the higher the geothermal gradient, the lower the difference between the temperatures in question. This indicates that the geothermal gradient was high during the late Variscan or post-Variscan deformation/thermal pulse and was related to the migration of hydrothermal solutions. The discrepancy between both temperatures may be explained by the small impact (i.e., low thermal capacity) of these solutions and/or the relatively short influence time on OM. The calcite veins are very thin and were probably developed in a short time. A high amount of primary FIAs confirms the fast growth of calcite (Roedder, 1984; Goldstein and Reynolds, 1994).

In the eastern part (quartz samples CZ74 and SV), a small amount of primary FIAs, which occupy small areas in crystals, and a large amount of secondary inclusions indicate that the quartz veins underwent tectonic disturbances. This was responsible for the cracking of crystals and re-crystallisation along the crack paths. In the preserved areas of primary FIAs, stress could facilitate swelling and the unsealing processes of inclusions. It is also possible that the migration of solutions took place in heterogeneous conditions or that they underwent necking down after a phase change (Goldstein, 2001). Moreover, heterogeneous conditions of fluid migration are supported by the high variability of CH_4 contents in inclusions. Both cases (swelling and unsealing, as well as heterogeneous conditions) result in a wide range of homogenisation temperatures. Therefore, in the case of samples Cz74 and SV, the quality of fluid inclusion data does not permit the calculation of a geothermal palaeogradient. However, fluid inclusion data indicate that

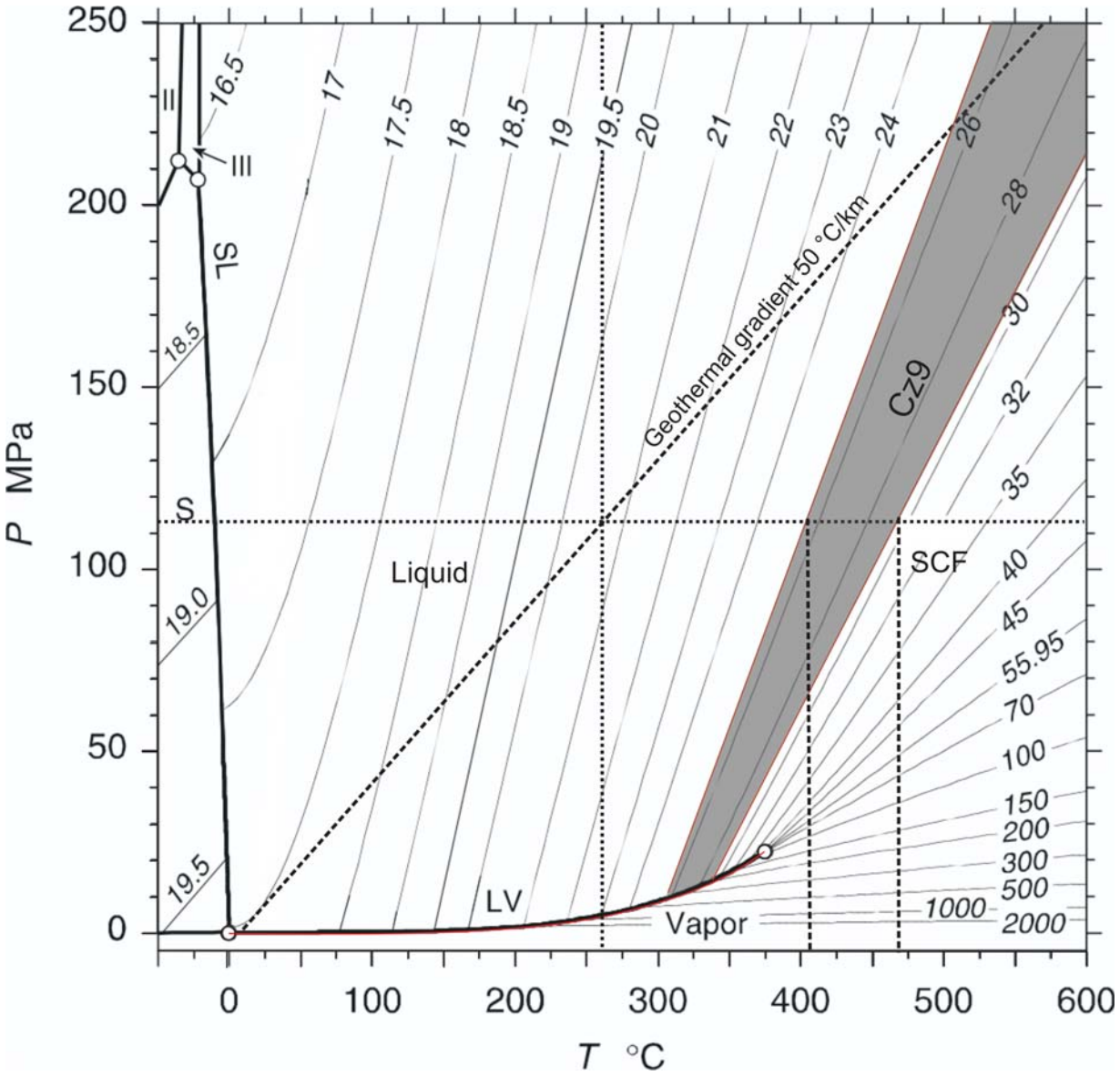

Fig. 12. P-T diagram with marginal isochores of H_2O from an inclusion in sample Cz9 (calculation after Diamond, 2003; Bakker, 2009, 2012).

fluid migration occurred at greater depths. In the Upper Silesian Coal Basin, the calculated heat flow for maximum burial in the late Carboniferous is 75–80 mW/m^2 (Geršlová *et al.*, 2016), which corresponds to geothermal gradient of ~40 °C/km. The Upper Silesian Coal Basin is a distal part of the Variscan foreland; therefore, a lower geothermal gradient can be expected by comparison with the Moravo-Silesian Culm Basin.

Previous studies on fluid inclusions in the Culm Basin (Zimák *et al.*, 2002; Kučera *et al.*, 2010; Dolníček *et al.*, 2014) focused on veins associated with ore mineralisation. Their homogenisation temperatures are considerably lower than those of samples CZ9, CZ74 and SV. These authors did not detect any inclusions with a high molar volume of CO_2, contrary to sample CZ54 of the present study. In turn, all the samples considered here do not have even a trace of ore minerals. In conclusion, these samples must represent a different kind of vein, formed earlier under deep burial conditions and from a different type of fluid, compared to those related to later ore mineralisation.

Mineralogy of high-grade samples

The samples showing the highest Raman-derived palaeotemperature (POK2 and ZLH), from the NW part of the study area also were studied through microscope observation of the rock fabrics in thin sections and X-ray diffraction analysis of the mineralogical composition (S. Kowalska, *unpub. data*). On the microscopic scale, two generations of metamorphic foliation are clearly visible in the most thermally mature samples: in the first step, slaty cleavage (S_1) was developed and after that a crenulation process took place (S_2). This multiple fabric could indicate deformation at a temperature of at least ~350 °C (Dunlap, 1997). The mineralogical composition of the samples analysed is very simple. It consists mainly of chlorites, illite and muscovite,

quartz and albite (S. Kowalska, *unpub. data*). However, biotite was not found in the material studied. The maximum palaeotemperatures were estimated from the illite crystallinity – the Kübler index, according to the methodology proposed by Warr and Rice (1994) with the correction of Warr and Mahlmann (2015). The achieved Kübler Index (calibrated to the CIS scale) is equal to 0.26 Δ°2θ (glycolated preparation) and indicates maximum palaeotemperatures of about ~350 ± 30 °C. This means that the metamorphism reached epizone conditions. Taking into account these mineralogical data, it appears that the Raman-derived temperature of the samples ZLH (T_{RSOM} 394 °C) and POK2 (T_{RSOM} 389 °C) is slightly overestimated.

Regional context

A dominant feature of the eastern margin of the Bohemian Massif, particularly in the Moravo-Silesian Zone, is the constant kinematics that indicate top-to-the-NE-oriented transpressive movements, consistent with oblique collision (Cháb *et al.*, 1990; Schulmann and Gayer 2000). The sequence of structural events, ranging from early-metamorphic folding and foliation development, to post-metamorphic shearing, is related to nappe exhumation and late orogenic extension and it is also a feature common to the MSFTB. In the metamorphic western part of the Moravo-Silesian Zone (west of the Culm Basin), another characteristic feature is a metamorphic zonation that ranges from chlorite zone in the east to kyanite-sillimanite zones in the west. The metamorphic zones are tectonically inverted, so that the highest metamorphic grade occurs at the top of the nappe sequence. The isograds trend NE-SW, cross-cutting the lithological boundaries (Cháb *et al.*, 1990; Schulmann and Gayer, 2000). This zonation indicates a westward temperature and pressure increase from 300–350 °C at 2–3 kbar in the east (close to the western end of the Culm Basin) to 600 °C at pressures of <6 kbar in the west (Cháb *et al.*, 1990).

The formation of narrow grabens (e.g., Boskovice Furrow) filled with Stephanian to Autunian sediments in front of the crystalline nappes indicates postorogenic extension of overthickened Variscan orogenic crust (Grygar and Vavro, 1995; Jelínek *et al.*, 2003; Kalvoda *et al.*, 2008). The possible post-collisional extension may be also indicated by the intrusions of basaltic dykes into the Permian sediments (Kalvoda *et al.*, 2008).

The palaeomagnetic studies in the Orlica-Śnieżnik Dome and Kłodzko Metamorphic Complex, carried out west of the study area (Kądziałko-Hofmokl *et al.*, 2003, 2013 and references therein), showed a significant remagnetisation episode in the Mesozoic (with a peak in the Triassic–Jurassic), which might have been associated with hydrothermal activity. However, the palaeomagnetic data of Tait *et al.* (1996) and Grabowski *et al.* (2009) for the Devonian carbonates from the eastern part of the Moravo-Silesian Zone (Hranice and Drahany Upland area) mainly indicate the late Carboniferous age of remagnetisation. This palaeomagnetic data pattern is similar to the organic maturity data and ZHe dating of the present study. It coincides well with the maturity development in the Polish part of the Moravo-Silesian Zone (Kotas, 1971; Kotas *et al.*, 1983; Bełka, 1993; Środoń *et al.*, 2006; Botor, 2014), as well as with the timing of some principal tectonomagmatic processes at the eastern margin of the Bohemian Massif (Bábek *et al.*, 2005). These include late Carboniferous ages of the Žulová intrusive body, major remagnetisation events in the Drahany Upland and eastern part of the Nízký Jeseník Basin (Chadima *et al.*, 2006; Grabowski *et al.*, 2009) and ~300 Ma mica cooling ages in the Keprník and Desná domes (Maluski *et al.*, 1993).

A thermal event(s) of the Permian-Mesozoic age is also known from W and SW Poland (Środoń and Clauer, 2001; Środoń *et al.*, 2006; Środoń *et al.*, 2014; Turniak *et al.*, 2014; Kowalska *et al.*, 2015). In the Carboniferous substratum of the Fore-Sudetic Monocline, a Late Permian to Early Jurassic thermal event(s) has also been established recently from illite K-Ar and ZHe dating (Kowalska *et al.*, 2015) and also was indicated by thermal maturity modelling (Botor *et al.*, 2013). Similar conclusions were given by Środoń *et al.*, (2014) considering the thermal evolution of the Triassic strata in the Silesian-Cracow Monocline. Triassic K-Ar ages (234 to 226 Ma) from post-uranium stage illite in the Rožná deposit (Kříbek *et al.*, 2009) and Early–Middle Jurassic ZHe cooling ages (194.1 to 162.9 Ma) from the western part of the Culm Basin (D. Botor, *unpub. data*) are consistent with the early Tethys-Central Atlantic rifting and tectonic reactivation of the Variscan structures of the Bohemian Massif. Summing up, several lines of evidence confirmed the post-Variscan extensional development of the area located NE of the Bohemian Massif (Grygar and Vavro, 1995; Kalvoda, 1998; Turniak *et al.*, 2014; Kowalska *et al.*, 2015). The extensional regime might have caused a high heat flux in the crust and advective heat transport due to the circulation of hot fluids. Consequently, it caused overprinting of the former burial-related maturation of OM. It is also possible that several extensional phases developed between the Permian and Jurassic time.

CONCLUSIONS

Applying combined Raman spectroscopy of OM, vitrinite reflectance and fluid inclusions data, the maximum palaeotemperatures of the lower Carboniferous siliciclastic rocks of the Moravo-Silesian Culm Basin in the Nízký Jeseník Mts. were estimated. The Raman-derived maximum palaeotemperatures vary from ~200 ± 30 °C in the E to ~350 ± 30 °C in the W. This is in agreement with the burial-related temperatures in the E and with the hydrothermally related temperatures in the central and western parts of the basin. The thermal maturity pattern in the lower Carboniferous Culm Basin of the Nízký Jeseník area is explained by: (1) Variscan (mid–late Carboniferous) burial diagenesis in the eastern part of the basin and (2) post-Variscan, probably Permian and/or Mesozoic (presumably Triassic), thermal pulse(s) probably related to advective heat transport by circulating fluids that presumably overprinted the Variscan metamorphism in the central and western part of the basin. The results prove that Variscan convergence, which ceased in the late Carboniferous, was later (early Permian onwards) replaced by an extensional regime, as suggested by Grygar and Vavro (1995) and Turniak *et al.* (2014). Additionally,

this work shows that the Raman spectra-fitting procedure and the estimation of metamorphic temperature, proposed by Kouketsu *et al.* (2014), are suitable techniques, which can be applied successfully to thermal studies in a variety of tectonic settings.

Acknowledgements

We would like to express our gratitude to the journal reviewers, Ondřej Bábek and Mirosław Słowakiewicz, and to Editor Stanisław Mazur for their valuable input, which significantly improved the quality of the paper. Our thanks also go to Paweł Filipiak (University of Silesia, Sosnowiec) for checking the organic maturity by applying palynological investigations on selected samples, Sylwia Kowalska for rock fabrics and XRD data, Marian Wagner for discussing some aspects of organic petrology, Barbara Kwiecińska for reading the early version of the manuscript and her remarks, Andrzej Skowroński (the latter three of AGH-UST, Kraków) and Frank Simpson for language correction. The research was partially funded by AGH Statutory Projects 11.11.140.562 and 11.11.140.320.

REFERENCES

Aoya, M., Kouketsu, Y., Endo, S., Shimizu, H., Mizukami, T., Nakamura, D. & Wallis, S., 2010. Extending the applicability of the Raman carbonaceous material geothermometer using data from contact metamorphic rocks. *Journal of Metamorphic Geology*, 28: 895–914.

Bábek, O. & Franců, E., 2004. Regional trends in thermal maturity of Paleozoic rocks of the Moravo-Silesian Basin: a combined study of Conodont Alteration Index (CAI), vitrinite reflectance and Rock-Eval pyrolysis. *GeoLines*, 17: 16–17.

Bábek, O., Franců, E., Kalvoda, J. & Neubauer, F., 2008. A digital image analysis approach to measurement of the conodont colour alteration index (CAI): a case study from the Moravo-Silesian Zone, Czech Republic. *Neues Jahrbuch für Geologie und Paläontologie, Abhandlungen*, 249: 185–201.

Bábek, O., Mikuláš, R., Zapletal, J. & Lehotský, T., 2004. Combined tectonic-sediment supply driven cycles in a Lower Carboniferous deep-marine foreland basin, Moravice Formation, Czech Republic. *International Journal of Earth Sciences*, 93: 241–261.

Bábek, O., Tomek, C., Melichar, R., Kalvoda, J. & Otava, J., 2006. Structure of unmetamorphosed Variscan tectonic units of the southern Moravo-Silesian Massif: a review. *Neues Jahrbuch für Geologie und Paläontologie, Abhandlungen*, 239: 37–75.

Bábek, O., Tomek, C., Neubauer, F., Franců, E., Kalvoda, J. & Franců, E., 2005. Thermal overprint in Paleozoic sediments of the Moravo-Silesian Zone, Bohemian Massif: a record of late Variscan orogen-parallel extension. *GeoLines*, 19: 17.

Bakker, R. J., 2009. Package FLUIDS. Part 3: correlations between equations of state, thermodynamics and fluid inclusions. *Geofluids*, 9: 63–74.

Bakker, R. J., 2012. Package FLUIDS. Part 4: thermodynamic modelling and purely empirical equations for H_2O-NaCl-KCl solutions. *Mineralogy and Petrology*, 105: 1–29.

Barker, C., Pawlewicz, M. J., 1994. Calculation of vitrinite reflectance from thermal histories: a comparison of methods. In: Mukhopadhyay, P. K. & Dow, W. G. (eds), Vitrinite reflectance as a maturity parameter: applications and limitations. American Chemical Society Symposium Series, 570: pp. 216–229.

Barzoi, S. C., 2015. Shear stress in the graphitization of carbonaceous matter during the low-grade metamorphism from the northern Parang Mountains (South Carpathians) — Implications to graphite geothermometry. *International Journal of Coal Geology*, 146: 179–187.

Bełka, Z., 1993. Thermal and burial history of the Cracow–Silesia region (southern Poland) assessed by conodont CAI analysis. *Tectonophysics*, 227: 161–190.

Beny-Bassez, C. & Rouzaud, J. N., 1985. Characterisation of carbonaceous materials by correlated electron and optical microscopy and Raman microspectrometry. *Scanning Electron Microscopy,* 1: 119–132.

Beyssac, O., Brunet, F., Petitet, J., Goffé, B. & Rouzaud, J. N., 2003a. Experimental study of the microtextural and structural transformations of carbonaceous materials under pressure and temperature. *European Journal of Mineralogy,* 15: 937–951.

Beyssac, O, Goffe, B., Chopin, C. & Rouzaud, J. N., 2002a. Raman spectra of carbonaceous material in metasediments; a new geothermometer. *Journal of Metamorphic Geology*, 20: 858–871.

Beyssac, O., Goffe, B., Petitet, J. P., Froigneux, E., Moreau, M. & Rouzaud, J. N., 2003b. On the characterization of disordered and heterogeneous carbonaceous materials by Raman spectroscopy. *Spectrochimica Acta Part A: Molecular and Bio-molecular Spectroscopy*, 59: 2267–2276.

Beyssac, O., Rouzaud, J. N., Goffé, B., Brunet, F. & Chopin, C., 2002b. Graphitization in a high-pressure, low-temperature metamorphic gradient: A Raman microspectroscopy and HRTEM study. *Contributions to Mineralogy and Petrology*, 143: 19–31.

Botor, D., 2010. Organic maturity of the Mesozoic strata of the overburden of the Upper Silesia Coal Basin. In: Lipiarski, I. (ed.), *Materiały Sympozjum: Geologia Formacji Węglonośnych Polski*, *Kraków, 21-22 kwietnia 2010.* Akademia Górniczo-Hutnicza im. S. Staszica, Wydział Geologii, Geofizyki i Ochrony Środowiska, Kraków, pp. 42–46. [In Polish, with English summary.]

Botor, D., 2014. Timing of coalification of the Upper Carboniferous sediments in the Upper Silesia Coal Basin on the basis of by apatite fission track and helium dating. *Gospodarka Surowcami Mineralnymi — Mineral Resources Management,* 30: 85–104. [In Polish, with English summary.]

Botor, D., Papiernik, B., Maćkowski, T., Reicher, B., Kosakowski, P., Machowski, G. & Górecki W., 2013. Gas generation in the Carboniferous source rocks of the Variscan and their foreland: implications for a charge history of natural gases of the Rotliegend deposits. *Annales Societatis Geologorum Poloniae,* 83: 353–383.

Bruns, B. & Littke, R., 2015. Lithological dependency and anisotropy of vitrinite reflectance in high rank sedimentary rocks of the Ibbenbüren area, NW Germany: Implications for the tectonic and thermal evolution of the Lower Saxony Basin. *International Journal of Coal Geology*, 137: 124–135.

Burke, E. A. J., 2001. Raman microspectrometry of fluid inclusions. *Lithos*, 55: 139–158.

Bustin, R. M., Ross, J. V. & Moffat, I., 1986. Vitrinite anisotropy under differential stress and high confining pressure and temperature: preliminary observations. *International Journal of Coal Geology*, 6: 343–351.

Cháb, J., Fediuková, E., Fisera, M., Novotny, P. & Opletal, M., 1990. Variscan orogeny in the Silesicum. *Sbornik geologickych ved, Ložisková geologie, mineralogie*, 29: 9–39. [In Czech, with English summary.]

Chadima, M., Hrouda, F. & Melichar, R., 2006. Magnetic fabric study of the SE Rhenohercynian Zone (Bohemian Massif):

Implications for dynamics of the Paleozoic accretionary wedge. *Tectonophysics*, 418: 93–109.

Čížek, P. & Tomek, C., 1991. Large-scale thin-skinned tectonics in the Eastern boundary of the Bohemian Massif. *Tectonics*, 10: 273–286.

Dallmeyer, R. D., Franke, W. & Weber, K., 1995. *Pre-Permian Geology of Central and Eastern Europe*. Springer, Berlin, 609 pp.

Dallmeyer, R. D., Neubauer, F. & Hock, V., 1992. Chronology of late Paleozoic tectonothermal activity in the southeastern Bohemian Massif, Austria (Moldanubian and Moravo-Silesian zones): 40Ar/39Ar mineral age controls. *Tectonophysics*, 210: 135–153.

Danišík, M., Štěpančiková, P. & Evans, N. J., 2012. Constraining long-term denudation and faulting history in intraplate regions by multi-system thermochronology – an example of the Sudetic Marginal Fault (Bohemian Massif, Central Europe). *Tectonics*, 31: 1–19.

Diamond, L. W., 2001. Review of the systematics of CO_2–H_2O fluid inclusions. *Lithos*, 55: 69–99.

Diamond, L. W., 2003. Systematics of H_2O inclusions. In: Samson, I., Anderson, A. & Marshall, D. (eds), Fluid inclusions: Analysis and interpretation. *Mineralogical Association of Canada Short Course Series*, 32: 55–79.

Diessel, C. F. K., Brothers, R. N. & Black, P. M., 1978. Coalification and graphitization in high-pressure schists in New Caledonia. *Contributions to Mineral Petrology*, 68: 63–78.

Diessel, C. F. K. & Offler, R., 1975. Change in physical properties of coalified and graphitised phytoclasts with grade of metamorphism. *Neues Jahrbuch für Mineralogie, Monatshefte,* 1975(3): 11–26.

Dolníček, Z., Lehotský, T., Slobodník, M., Hejtmánková, E., Grígelová, A. & Zapletal, J., 2014. Mineral-forming and diagenetic processes related to Tertiary hydrocarbon seepage at the Bohemian Massif/Outer Western Carpathians interface: Evidence from the Hrabuvka quarry, Moravia, Czech Republic. *Marine and Petroleum Geology*, 52: 77–92.

Dudek, A., 1980. The crystalline basement block of the Outer Carpathians in Moravia: Bruno-Vistulicum. *Rozpravy České akademie věd, Třída Mathematicko-Přírodovědecká*, 90: 1–85.

Dunlap, W. J., 1997. Neocrystallization or cooling? $^{40}Ar/^{39}Ar$ ages of white micas from low-grade mylonites. *Chemical Geology*, 143: 181–203.

Dvořák, J., 1973. Synsedimentary tectonics of the Paleozoic of the Drahany Upland (Sudeticum, Moravia, Czechoslovakia). *Tectonophysics*, 17: 359–391.

Dvořák, J., 1989. Anchimetamorphism in the Variscan tectogene in Central Europe – its relationship to tectogenesis. *Věstník Ústredního Ústavu Geologického*, 64: 17–30. [In Czech, with English abstract.]

Dvořák, J., 1994. Variscan flysch evolution of the Nízký Jeseník Mts. in Moravia and Silesia. *Czech Geological Survey Special Papers*, 3. Prague, 77 pp. [In Czech, with English summary.]

Dvořák, J. & Paproth, E., 1969. Über die Position und die Tektogenese des Rhenoherzynikums und des Sudetikums in den mitteleuropäischen Varisziden. *Neues Jahrbuch für Geologie und Paläontologie, Monatshefte*, 1969(2): 65–88.

Dvořák, J., Honek, J., Pesek, J. & Valterova, P., 1997. Deep borehole evidence for a southward extension of the Early Namurian deposits near Nemcicky, S. Moravia, Czech Republic: implication for rapid coalification. In: Gayer, R. & Pesek, J. (eds), *European Coal Geology and Technology. Geological Society, London, Special Publication*, 125: 179–193.

Dvořák, J. & Wolf, M., 1979. Thermal metamorphism in the Moravian Paleozoic (Sudeticum, CSSR). *Neues Jahrbuch für Geologie und Paläontologie, Monatshefte*,1979(10): 596–607.

Fojt, B. & Vecera J., 2000. Zlate Hory ve Slezku — jajvetsi rudni revir v Jesenikach. *Acta Museum Moraviae, Scientiae Geologicae*, 86: 3–35. [In Czech.]

Ferrari, A. C. & Robertson, J., 2000. Interpretation of Raman spectra of disordered and amorphous carbon. *Physical Review B*, 61: 95–107.

Franců, E., Franců, J. & Kalvoda, J., 1999. Illite crystallinity and vitrinite reflectance in Paleozoic siliciclastics in the SE Bohemian Massif as evidence of thermal history. *Geologica Carpathica*, 50: 365–372.

Franců, E., Franců, J., Kalvoda, J., Polcheau, H. S. & Otava, J., 2002. Burial and uplift history of the Palaeozoic Flysch in the Variscan foreland basin (SE Bohemian Massif, Czech Republic). *EGS Stephen Mueller Special Publication Series*, 1: 259–278.

Franke, W., 1995. Rhenohercynian foldbelt; Autochthon and nonmetamorphic nappe units: stratigraphy. In: Dallmeyer, R. D., Franke, W. & Weber K. (eds), *Pre-Permian Geology of Central and Eastern Europe*. Springer, Berlin, pp. 33–49.

Franke, W. & Żelaźniewicz, A., 2000. The eastern termination of the Variscides: terrane correlation and kinematic evolution. In: Franke, W., Haak, V., Oncken, O. & Tanner, D. (eds), *Orogenic processes quantification and modelling in the Variscan Belt. Geological Society, London, Special Publications*, 179: pp. 63–86.

Fritz, H. & Neubauer, F., 1995. Moravo-Silesian Zone: Autochthon – structure. In: Dallmeyer, R. D., Franke, W. & Weber, K. (eds), *Pre-Permian Geology of Central and Eastern Europe*. Springer, Berlin, pp. 490–494.

Geršlová, E., Goldbach, M., Geršl, M. & Skupien, P., 2016. Heat flow evolution, subsidence and erosion in Upper Silesian Coal Basin, Czech Republic. *International Journal of Coal Geology*, 154–155: 30–42.

Goldstein, R. H., 2001. Fluid inclusions in sedimentary and diagenetic systems. *Lithos*, 55: 159–193.

Goldstein, R. H. & Reynolds, T. J., 1994. *Systematics of fluid inclusions in diagenetic minerals.* Society for Sedimentary Geology Short Course, 31, 199 pp. Tulsa, USA.

Grabowski, J., Bábek, O., Hladil, J., Pruner, P., Schnabl, P., Werner, T., Gersl, M. & Otava, J., 2009. Late Variscan remagnetization of Devonian carbonates in the Moravo-Silesian zone (Czech Republic): implications for dating tectonic deformation. *Trabajos de Geología*, 29: 315–320.

Grygar, R. & Vavro, M., 1995. Evolution of Lugosilesian Orocline (north-eastern periphery of the Bohemian Massif): Kinematics of Variscan deformation. *Journal of Czech Geological Society*, 40: 65–90.

Guedes, A., Valentim, B., Prieto, A. C., Rodrigues, S. & Noronha, F., 2010. Micro-Raman spectroscopy of collotelinite, fusinite and macrinite. *International Journal of Coal Geology*, 83: 415–422.

Hackley, P .C., Araujo, C. V., Borrego, A. G., Bouzinos, A., Cardott, B. J., Cook, A. C., Eble, C., Flores, D., Gentzis, T., Gonçalves, P. A., Mendonça Filho, J. G., Hámor-Vidó, M., Jelonek, I., Kommeren, K., Knowles, W., Kus, J., Mastalerz, M., Menezes T. R., Newman, J., Oikonomopoulos, J. K., Pawlewicz, M., Pickel, W., Potter, J., Ranasinghe, P., Read, H., Reyes, J., De La Rosa Rodriguez, G., de Souza, I. V. A. F., Suárez-Ruiz, I., Sýkorová I. & Valentine, B. J., 2015. Standardization of reflectance measurements in dispersed organic matter: Results of an exercise to improve interlaboratory agreement. *Marine and Petroleum Geology*, 59: 22–34.

Hartkopf-Fröder, C., Königshof, P., Littke, R. & Schwarzbauer, J., 2015. Optical thermal maturity parameters and organic geo-

chemical alteration at low-grade diagenesis to anchimetamorphism: A review. *International Journal of Coal Geology*, 150–151: 74–119.

Hartley, A. J. & Otava, J., 2001. Sediment provenance and dispersal in a deep marine foreland basin: The Lower Carboniferous Culm Basin, Czech Republic. *Journal of the Geological Society, London*, 158: 137–150.

Hinrichs, R., Brown, M. T., Vasconcellos, M. A. Z., Abrashev, M. V. & Kalkreuth, W., 2014. Simple procedure for an estimation of the coal rank using micro-Raman spectroscopy. *International Journal of Coal Geology*, 136: 52–58.

Hladil, J., 1994. Moravian middle and late Devonian buildups: evolution in time and space with respect to the Laurussian shelf. *Courier Forschungsinstitut Senckenberg*, 172: 111–125.

Hladil, J., Melichar, R., Otava, J., Galle, A., Krs, M., Man, O., Pruner, P., Cejchan, P. & Orel, P., 1999. The Devonian in the Easternmost Variscides, Moravia; a holistic analysis directed towards comprehension of the original context. *Abhandlungen der Geologischen Bundesanstalt, Wien*, 54: 27–47.

Janiková, P., Stary, J., Klika, R., Kavina, P., Jirásek, J. & Sivek M., 2015. Gold deposits of the Czech Republic from a mineral policy perspective. *Gospodarka Surowcami Mineralnymi — Mineral Resources Management*, 31: 35–50.

Jehlička, J. & Rouzaud, J. N., 1990. Organic geochemistry of Precambrian shales and schists (Bohemian massif, Central Europe). *Organic Geochemistry*, 16: 865–872.

Jehlička, J., Urban, O. & Pokorný, J., 2003. Raman spectroscopy of carbon and solid bitumens in sedimentary and metamorphic rocks. *Spectrochimica Acta, Part A*, 59: 2341–2352.

Jelínek, F., Leichmann, J. & Nehyba, S., 2003. Conglomerates of the Boskovice Furrow — indicator of tectonic evolution of the eastern margin of the Bohemian Massif. *Journal of the Czech Geological Society*, 48: 74–75.

Jirásek, J., Wlosok, J., Sivek, M., Matýsek, D., Schmitz, M., Sýkorová, I. & Vašíček, Z., 2014. U-Pb zircon age of the Krásné Loučky tuffite: the dating of Visean flysch in the Moravo–Silesian Paleozoic Basin (Rhenohercynian Zone, Czech Republic). *Geological Quarterly*, 58: 659–672.

Jurczak-Drabek, A., 1996. *Coal Quality Atlas of the Upper Silesia Coal Basin*. Państwowy Instytut Geologiczny, Warsaw. [In Polish, with English summary.]

Kalvoda, J., 1998. The main phases of extension in the eastern part of the Rhenohercynian Zone. *Acta Universitatis Carolinae, Geologica*, 42: 274–275.

Kalvoda, J. & Melichar, R., 1999. Paleozoic sediments of the Drahany Upland. *Geolines* 8: 88–90.

Kalvoda, J., Bábek, O., Fatka, O., Leichmann, J., Melichar, R., Nehyba, S. & Špacek, P., 2008. Brunovistulian terrane (Bohemian Massif, Central Europe) from late Proterozoic to late Paleozoic: a review. *International Journal of Earth Sciences*, 97: 497–518.

Kandarachevová, J., Sedláčková, L., Hýlová., L, Jirásek., J. & Sivek, M., 2009. Lateral development of coalification in the Czech part of the Upper Silesian Coal Basin and its connection with gas deposits. *International Journal of Coal Geology*, 78: 225–232.

Katagiri, G., Ishida, H. & Ishitani A., 1988. Raman spectra of graphite edge planes. *Carbon*, 26: 565–71.

Kądziałko-Hofmokl, M., Kruczyk, J., Mazur, S. & Siemiątkowski, J., 2003. Paleomagnetism of the Upper Proterozoic and Devonian rocks from the Kłodzko Metamorphic Complex in the West Sudetes (SW Poland): tectonic implications for the Variscan belt of Central Europe. *Tectonophysics*, 377: 83–99.

Kądziałko-Hofmokl, M., Szczepański, J., Werner, T., Jeleńska, M. & Nejbert, K., 2013. Paleomagnetism and magnetic mineralogy of metabasites and granulites from Orlica-Śnieżnik Dome (Central Sudetes). *Acta Geophysica*, 61: 535–568.

Kędzior, S., 2009. Accumulation of coalbed methane in the southwest part of the Upper Silesian Coal Basin (southern Poland). *International Journal of Coal Geology*, 80: 20–34.

Kędzior, S., 2015. Methane contents and coal-rank variability in the Upper Silesian Coal Basin, Poland. *International Journal of Coal Geology*, 139: 152–164.

Kościówko, H., 1982. *Mapa Geologiczna Polski (1:200 000) – Ark. Nysa*. Wydawnictwa Geologiczne Warszawa. [In Polish.]

Kotas, A., 1971. Remarques sur le métamorphisme du charbon du Bassin Houiller de Haute Sielésie. *Zeszyty Naukowe AGH, Seria Geologia*, 14: 7–25. [In Polish, with French abstract.]

Kotas, A., Gądek, S., Buła, Z., Kwarciński, J. & Malicki, J., 1983. *Geological atlas of the Upper Silesia Coal Basin, Poland. Part II. Coal Quality Maps (1: 100 000)*. Geological Institute, Warszawa. [In Polish, with English abstract.]

Kouketsu, Y., Mizukami, T., Mori, H., Endo, S., Aoya, M., Hara, H., Nakamura, D. & Wallis, S., 2014. A new approach to develop the Raman carbonaceous material geothermometer for low-grade metamorphism using peak width. *Island Arc*, 23: 33–50.

Kowalska, S., Wolański, K., Botor, D., Dunkl, I., Wojtowicz, A., Jonkisz, U. & Buniak, A., 2015. Complex thermal history reconstruction of Carboniferous rocks from the Fore-Sudetic Monocline — application in a tight gas exploration of illite K-Ar and zircon helium dating. *EuroClay Conference, Edinburgh 5th-10th July 2015.* Programme & Abstracts, The Clay Minerals Society, Edinburgh, p. 428.

Kříbek, B., Žák, K., Dobeš, P., Leichmann, J., Pudilová, M., René, M., Scharm, B., Scharmová, M., Hájek, A., Holeczy, D., Hein, U. F. & Lehmann, B., 2009. The Rožná uranium deposit (Bohemian Massif, Czech Republic): shear zone-hosted, late Variscan and post-Variscan hydrothermal mineralization. *Mineralia Deposita*, 44: 99–128.

Kučera, J., Muchez, P., Slobodnik, M. & Prochaska, W., 2010. Geochemistry of highly saline fluids in siliciclastic sequences: genetic implications for post-Variscan fluid flow in the Moravo-Silesian Palaeozoic of the Czech Republic. *International Journal of Earth Sciences*, 99: 269–284.

Kučera, J. & Slobodnik, M., 2002. Regional extension of hydrothermal veins – result of an important deformation event in the Moravosilesian Paleozoic. *Geolines*, 14: 55.

Kumpera, O., 1983. *Geologie spodního karbonu jesenického bloku.* Ústední ústav geologický, Praha. [In Czech.]

Kumpera, O. & Martinec, P., 1995. The development of the Carboniferous accretionary wedge in the Moravian-Silesian Paleozoic Basin. *Journal of the Czech Geological Society*, 40: 47–64.

Kwiecińska, B. & Petersen, H. I., 2004. Graphite, semi-graphite, natural coke, and natural char classification — ICCP system. *International Journal of Coal Geology*, 57: 99–116.

Kwiecińska, B., Suárez-Ruiz, I., Paluszkiewicz, C. & Rodriques, S., 2010. Raman spectroscopy of selected carbonaceous samples. *International Journal of Coal Geology*, 84: 206–212.

Lahfid, A., Beyssac, O., Deville, E., Negro, F., Chopin, C. & Goffé, B., 2010. Evolution of the Raman spectrum of carbonaceous material in low-grade metasediments of the Glarus Alps (Switzerland). *Terra Nova*, 22: 354–360.

Le Bayon, R., 2012. Laboratory organic matter maturation at high pressures: heat-up effect on vitrinite reflectance. *Swiss Journal of Geosciences*, 105: 171–181.

Le Bayon, R., Adam, C. & Mählmann, R. F., 2012. Experimentally determined pressure effect on vitrinite reflectance at 450 °C. *International Journal of Coal Geology*, 92: 69–81.

Littke, R., Urai, J. L., Uffmann, A. K. & Risvanis, F., 2012. Reflectance of dispersed vitrinite in Palaeozoic rocks with and without cleavage: Implications for burial and thermal history modeling in the Devonian of Rursee area, northern Rhenish Massif, Germany. *International Journal of Coal Geology*, 89: 41–50.

Lünsdorf, N. K., 2016. Raman spectroscopy of dispersed vitrinite – Methodical aspects and correlation with reflectance. *International Journal of Coal Geology*, 153: 75–86.

Lünsdorf, N. K., Dunkl, I., Schmidt, B. C., Rantitsch, G. & von Eynatten, H., 2014. Towards a higher comparability of geothermometric data obtained by Raman spectroscopy of carbonaceous material. Part I: evaluation of biasing factors. *Geostandards and Geoanalitycal Research*, 38: 73–94.

Lünsdorf, N. K. & Lünsdorf, J. O., 2016. Evaluating Raman spectra of carbonaceous matter by automated, iterative curve-fitting. *International Journal of Coal Geology*, 160–161: 51–62.

Magara, K., 1978. *Compaction and fluid migration*. *Developments in Petroleum Science*, 9. Elsevier Scientific Publishing, Amsterdam, Oxford, New York, 330 pp.

Malkovský, M., 1987. The Mesozoic and Tertiary basins of the Bohemian Massif and their evolution. *Tectonophysics*, 137: 31–42.

Maluski, H, Rajlich, P. & Souček, J., 1993. Pre-Variscan, Variscan and early Alpine thermo-tectonic history on the northeastern Bohemian massif: an $^{40}Ar/^{39}Ar$ study. *Geologische Rundschau*, 84: 345–358.

Martinec P., Kožušníková, A., Jirásek, J., Sivek, M., 2005. *Atlas of Coal in the Czech Part of the Upper Silesian Basin*. Anagram, Ostrava, 64 pp. [In Czech, with English summary.]

Marynowski, L. & Wyszomirski, P., 2008. Organic geochemical evidences of early-diagenetic oxidation of the terrestrial organic matter during the Triassic arid and semi-arid climatic conditions. *Applied Geochemistry*, 23: 2612–2618.

Marynowski, L., Zatoń, M., Bernd, R. T., Simoneit, T., Otto, A., Jędrysek, M. O., Grelowski, C. & Kurkiewicz, S., 2007. Compositions, sources and depositional environments of organic matter from the Middle Jurassic clays of Poland. *Applied Geochemistry* 22: 2456–2485.

Matthews, M. J., Pimenta, M. A., Dresselhaus, G., Dresselhaus, M. S. & Endo, M., 1999. Origin of dispersive effects of the Raman D band in carbon materials. *Physical Review B*, 59: 6585–6588.

Mazur, S, Aleksandrowski, P, Kryza, R. & Oberc-Dziedzic, T., 2006. The Variscan Orogen in Poland. *Geological Quarterly*, 50: 89–118.

McCann, T., Pascal, C., Timmerman, M. J., Krzywiec, P., Lopez-Gomez, J., Wetzel, A., Krawczyk, C. M., Rieke, H. & Lamarche, J., 2006. Post-Variscan (end Carboniferous-Early Permian) basin evolution in Western and Central Europe. In: Gee, D. G. & Stephenson, R. A. (eds), *European lithosphere dynamics. Geological Society, London, Memoirs*, 32: 355–388.

Morga, R., 2011. Micro-Raman spectroscopy of carbonized semifusinite and fusinite. *International Journal of Coal Geology*, 87: 253–267.

Morga, R., 2014. Raman microspectroscopy of funginite from the Upper Silesian Coal Basin (Poland). *International Journal of Coal Geology*, 131: 65–70.

Mullis, J., Dubessy, J., Poty, B. & O'Neil, J., 1994. Fluid regimes during late stages of a continental collision: physical, chemical, and stable isotope measurements of fluid inclusions in fissure quartz from a geotraverse through the Central Alps, Switzerland. *Geochimica and Cosmochimica Acta*, 58: 2239–2267.

Nemanich, R. J. & Solin, S. A., 1979. First- and second-order Raman scattering from finite-size crystals of graphite. *Physical Review B*, 20: 392–401.

Neubauer, F. & Handler, R., 1999. Variscan orogeny in the eastern Alps and Bohemian massif: How do these units correlate? *Mitteilungen der Österreichischen Geologischen Gesellschaft*, 92: 35–59.

Nowak, G., 2003. Petrology of dispersed organic matter in the Late Paleozoic strata in SW Poland. *Cuprum*, 4 (29): 1–221. [In Polish, with English summary.]

Pasteris, J. D. & Wopenka, B., 1991. Raman spectra of graphite as indicates of degree of metamorphism. *Canadian Mineralogist*, 29: 1–9.

Pimenta, M. A., Dresselhaus, G., Dresselhaus, M. S., Cancado, L. G., Jorio, A. & Saito, R., 2007. Studying disorder in graphite-based systems by Raman spectroscopy. *Physical Chemistry Chemical Physics*, 9: 1276–1291.

Pócsik, I., Hundhausen, M., Koos, M. & Ley, L., 1998. Origin of the D peak in the Raman spectrum of microcrystalline graphite. *Journal of Non-Crystalline Solids*, 227–230: 1083–1086.

Potgieter-Vermaak, S., Maledi, N., Wagner, N., Van Heerden, J. H. P., Van Grieken, R. & Potgieter, J. H., 2011. Raman spectroscopy for the analysis of coal: a review. *Journal of Raman Spectroscopy*, 42: 123–129.

Pohl, W. L., 2011. *Economic Geology: Principles and Practice*. Wiley & Sons, Oxford, 535 pp.

Pouba, Z., 1996. *Geological Map of Czech Republic. List. Jesenik.* Czech Geological Survey, Praha.

Pusz, S., Borrego, A. G., Alvarez, D., Camean, I., du Cann, V., Duber, S., Kalkreuth, W., Komorek, J., Kus, J., Kwiecińska, B. K., Libera, M., Marques, M., Misz-Kennan, M., Morga, R., Rodrigues, S., Smędowski, Ł., Suarez-Ruiz, I. & Strzezik, J., 2014. Application of reflectance parameters in the estimation of the structural order of coals and carbonaceous materials. Precision and bias of measurements derived from the ICCP structural working group. *International Journal of Coal Geology*, 131: 147–161.

Rahl, J. M., Anderson, K. M., Brandon, M. T. & Fassoulas, C., 2005. Raman spectroscopic carbonaceous material thermometry of low-grade metamorphic rocks: Calibration and application to tectonic exhumation in Crete, Greece. *Earth and Planetary Science Letters*, 240: 339–354.

Rajlich, P., 1990. Strain and tectonic styles related to Variscan transpression and transtension in the Moravo–Silesian Culmian basin, Bohemian Massif, Czechoslovakia. *Tectonophysics*, 174: 351–367.

Rantitsch, G., Grogger, W., Teichert, C., Ebner, F., Hofer, C., Maurer, E. M., Schaffer, B. & Toth, M., 2004. Conversion of carbonaceous material to graphite within the Greywacke Zone of the Eastern Alps. *International Journal of Earth Sciences*, 93: 959–973.

Rantitsch, G., Lämmerer, W., Fisslthaler, E., Mitsche, S. & Kaltenböck, H., 2016. On the discrimination of semi-graphite and graphite by Raman spectroscopy. *International Journal of Coal Geology*, 159: 48–56.

Reich, S. & Thomsen, Ch., 2004. Raman spectroscopy of graphite. *Philosophical Transactions of the Royal Society, London*, 362: 2271–2288.

Rodrigues, S., Marques, M., Suárez-Ruiz, I., Camean, I., Flores, D. & Kwiecińska, B., 2013. Microstructural investigations of natural and synthetic graphites and semi-graphites. *International Journal of Coal Geology*, 111, 67–79.

Roedder, E., 1984. Fluid inclusions. In: Ribbe, P. H. (ed.), *Reviews in Mineralogy – Short Course Notes. Mineralogical Society of America*, 12, 644 pp. Chantilly, USA.

Roth, Z., 1996. *Geological Map of Czech Republic. List. Olomouc*. Czech Geological Survey. Praha.

Sadezky, A., Muckenhuber, H., Grothe, H., Niessner, R. & Pöschl, U., 2005. Raman microspectrometry of soot and related carbonaceous materials: spectral analysis and structural information. *Carbon* 43: 1731–1742.

Schulmann, K. & Gayer, R., 2000. A model for a continental accretionary wedge developed by oblique collision: the NE Bohemian Massif. *Journal of the Geological Society*, *London*, 157: 401–416.

Schulmann, K., Konopásek, J., Janoušek, V., Lexa, O., Lardeaux, J. M., Edel, J. B., Štípská, P. & Ulrych, S., 2009. Andean type Palaeozoic convergence in the Bohemian Massif. *Comptes Rendus – Geoscience*, 341: 266–286.

Schulmann, K., Ledru, P., Autran, A., Melka., R, Lardeaux, J. M., Urban, M. & Lobkowicz, M., 1991. Evolution of nappes in the eastern margin of the Bohemian massif: a kinematic interpretation. *Geologische Rundschau*, 80: 73–92.

Sivek, M., Čáslavský, M. & Jirásek, J., 2008. Applicability of Hilt's law to the Czech part of the Upper Silesian Coal Basin (Czech Republic). *International Journal of Coal Geology*, 73: 185–195.

Sobczyk, A., Danišík, M., Aleksandrowski, P. & Anczkiewicz, A., 2015. Post-Variscan cooling history of the central Western Sudetes (NE Bohemian Massif, Poland) constrained by apatite fission-track and zircon (U-Th)/He thermochronology. *Tectonophysics*, 649: 47–57.

Špacek, P., Bábek, O.,·Štepancíková, P., Švancara, J., Pazdírková, J. & Sedlácek, J., 2015. The Nysa-Morava Zone: an active tectonic domain with Late Cenozoic sedimentary grabens in the Western Carpathians foreland (NE Bohemian Massif). *International Journal of Earth Sciences*, 104: 963–990.

Środoń, J. & Clauer, N., 2001. Diagenetic history of Lower Paleozoic sediments in Pomerania traced across the Teisseyre-Tornquist tectonic zone using mixed-layer illite-smectite. *Clay Minerals*, 36: 15–27.

Środoń, J., Clauer, N., Banaś, M. & Wojtowicz, A., 2006. K-Ar evidence for a Mesozoic thermal event superimposed on burial diagenesis of the Upper Silesia Coal Basin. *Clay Minerals*, 41: 671–692.

Środoń, J., Szulc, J., Anczkiewicz, A., Jewuła, K., Banaś, M. & Marynowski, L., 2014. Weathering, sedimentary and diagenetic controls of mineral and geochemical characteristics of the vertebrate-bearing Silesian Keuper. *Clay Minerals*, 49: 569–594.

Suchý, V, Frey, M. & Wolf, M., 1997. Vitrinite reflectance and shear-induced graphitization in orogenic belts: A case study from the Kandersteg area, Helvetic Alps, Switzerland. *International Journal of Coal Geology*, 34: 1–20.

Suchý, V., Sýkorová, I., Melka, K., Filip, J. & Machovič, V., 2007. Illite crystallinity, maturation of organic matter and microstructural development associated with lowest-grade metamorphism of Neoproterozoic sediments in the Teplá-Barrandian Unit, Czech Rep. *Clay Minerals*, 42: 415–438.

Sweeney, J. J. & Burnham, A. K., 1990. Evaluation of a simple model of vitrinite reflectance based on chemical kinetics. *American Association of Petroleum Geologists Bulletin*, 74: 1559–1570.

Tait, J. A., Bachtadse, V. & Soffel, H., 1996. Eastern Variscan fold belt: Paleomagnetic evidence for oroclinal bending. *Geology*, 24: 871–874.

Taylor, G. H., Teichmüller, M., Davis, A., Diessel, C. F. K., Littke, R. & Robert, P., 1998. *Organic Petrology: A New Handbook Incorporating Some Revised Parts of Stach's Textbook of Coal Petrology*. Gebrüder Borntraeger, Berlin, 704 pp.

Teichmüller, M., 1987. Organic material and very low-grade metamorphism. In: Frey M. (ed.), *Low-Temperature Metamorphism*. Chapman and Hall, New York, pp. 114–161.

Tuinstra, F. & Koenig, J. L., 1970. Raman spectrum of graphite. *Journal of Chemistry & Physics*, 53: 1126–1130.

Turniak, K., Mazur S., Domańska-Siuda, J. & Szuszkiewicz, A., 2014. SHRIMP U-Pb zircon dating for granitoids from the Strzegom-Sobótka Massif, SW Poland: Constraints on the initial time of Permo–Mesozoic lithosphere thinning beneath Central Europe. *Lithos*, 208–209: 415–429.

Ulyanova, E. V., Molchanov, A. N., Prokhorov, I. Y. & Grinyov, V. G., 2014. Fine structure of Raman spectra in coals of different rank. *International Journal of Coal Geology*, 121: 37–43.

Unrug, R., 1966. L´évolution sédimentaire et tectonique du bassin hercynien de Moravie-Haute-Silésie. *Bulletin de la Société Géologique de France*, 7: 537–547. [In French.]

Unrug, R., 1977. Lower Carboniferous Flysch in the Głubczyce region. *Rocznik Polskiego Towarzystwa Geologicznego – Annales Societatis Geologorum Poloniae*, 47: 72–99. [In Polish, with English summary.]

Unrug, R. & Dembowski, Z., 1971. Diastrophic and sedimentary evolution of the Moravia-Silesia Basin. *Rocznik Polskiego Towarzystwa Geologicznego – Annales Societatis Geologorum Poloniae*, 41: 118–168. [In Polish, with English summary.]

Vamvaka, A., Siebel, W., Chen, F. & Rohrmüller, J., 2014. Apatite fission-track dating and low-temperature history of the Bavarian Forest (southern Bohemian Massif). *International Journal of Earth Sciences*, 103: 103–119.

Warr, L. N. & Mählmann, R. F., 2015. Recommendations for Kübler Index standarization. *Clay Minerals*, 50: 283–286.

Warr, L. N. & Rice, A. H. N., 1994. Inter-laboratory standardization and calibration of clay mineral crystallinity and crystallite size data. *Journal of Metamorphic Geology*, 12: 141–152.

Wilkins, R. W. T., Boudou, R., Sherwood, N. & Xiao, X., 2014. Thermal maturity evaluation of inertinites by Raman spectroscopy: the RaMM technique. *International Journal of Coal Geology*, 128–129: 143–152.

Wilkins, R. W. T., Wang, M., Gan, H. & Li, Z., 2015. A RaMM study of thermal maturity of dispersed organic matter in marine source rocks. *International Journal of Coal Geology*, 150–151: 252–264.

Wopenka, B. & Pasteris, J. D., 1993. Structural characterization of kerogens to granulite-facies graphite: Applicability of Raman microprobe spectroscopy. *American Mineralogist*, 78: 533–557.

Yalcin, M. N., Littke, R. & Schsenhofer, R. F., 1997. Thermal history of sedimentary basins. In: Welte, D. H., Horsfield, B. & Baker, D. R. (eds), *Petroleum and Basin Evolution*. Springer, Dordrecht, Heidelberg, London, pp. 71–168.

Zapletal, J., Dvořák, J. & Kumpera O., 1989. Stratigrafická klasifikace kulmu Nízkého Jeseníku. *Věsttník Ústředního Ústavu Geolologického*, 64: 243–250. [In Czech.]

Zimák J., Losos Z., Novotný P., Dobes P. & Hladíková, J., 2002. Study of vein carbonates and notes to the genesis of the hydrothermal mineralization in the Moravo-Silesian Culm. *Journal of Czech Geological Society*, 47: 111–122.